Review | Open Access

Energy Materials

Wang et al. Energy Mater. 2026, 6, 600097 DOI:10.20517/energymater.2026.112

Polyoxometalates and their derivatives: structural tuning of versatile electrocatalysts for water splitting

Tian Wang[1], Wei Wang[2], Mingyu Xuan[1], Xiaohui Ma[1], Abdelkader Labidi[3], Gaofeng Chen[1,*]

Keywords:
Polyoxometalates, water splitting, hydrogen evolution reaction, oxygen evolution reaction, energy conversion

Citation: Wang, T.; Wang, W.; Xuan, M.; Ma, X.; Labidi, A.; Chen, G. Polyoxometalates and their derivatives: structural tuning of versatile electrocatalysts for water splitting. *Energy Mater.* **2026**, *6*, 600097. https://dx.doi.org/10.20517/energymater.2026.112

Received: 7 May 2026
First Decision: 8 Jun 2026
Revised: 28 Jun 2026
Accepted: 23 Jul 2026
Published: 11 Aug 2026

Academic Editor:
Soo Young Kim
Copy Editor:
Fangling Lan
Production Editor:
Fangling Lan

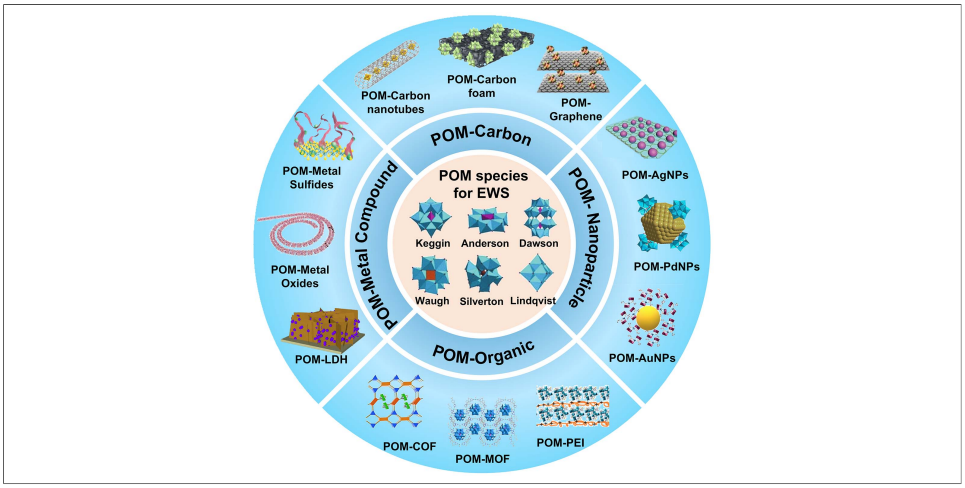

Abstract

Electrocatalytic water splitting is a promising energy-conversion technology for green hydrogen (H_2) production. However, the high cost and limited availability of noble-metal catalysts substantially impede its widespread commercialization. Polyoxometalates (POMs) and their derivatives have emerged as versatile and low-cost electrocatalytic alternatives due to their well-defined molecular structures, tunable active centers, reversible redox characteristics, and robust chemical stability. Most existing POM-related reviews merely focus broadly on generalized material applications or independently describe hydrogen evolution reaction (HER) and oxygen evolution reaction (OER) performance separately, without systematically addressing structural-tuning mechanisms or the quantitative catalytic advantages of POM-based water-splitting electrocatalysts. To fill this research gap, this review systematically summarizes the structure-activity relationship of typical POM frameworks (e.g., Keggin, Wells-Dawson, Anderson) for water splitting electrocatalysis. Representative POM-based composites and POM-derived metal compounds exhibit competitive catalytic performance: optimized POM-based electrodes can achieve overpotentials of 80-150 mV for the HER and 150-300 mV for the OER at a current density of 10 mA cm^{-2}. We comprehensively analyze the structural advantages of

[1]School of Environmental Engineering, Henan University of Technology, Zhengzhou 450001, Henan, China.
[2]State Key Laboratory of Materials Processing and Die & Mould Technology, School of Materials Science and Engineering, Huazhong University of Science and Technology, Wuhan 430074, Hubei, China.
[3]School of Environmental Science and Engineering, Shaanxi University of Science and Technology, Xi'an 710021, Shaanxi, China.

*Correspondence to: Dr. Gaofeng Chen, School of Environmental Engineering, Henan University of Technology, Zhengzhou 450001, Henan, China. E-mail: gaofengchen@haut.edu.cn

POMs in modulating electron transfer and optimizing reaction intermediate adsorption, and further discuss core limitations including insufficient intrinsic conductivity, particle aggregation, and structural dissolution during electrocatalysis. Finally, targeted structural tuning and composite engineering strategies are proposed to advance the development of high-performance, versatile POM-based electrocatalysts for efficient water splitting.

INTRODUCTION

The energy crisis and environmental degradation have driven advances in clean-energy conversion technologies. Hydrogen (H_2), recognized for its substantial energy density and lack of carbon emissions, stands out as a promising substitute for fossil fuels[1,2]. Electrocatalytic water splitting (EWS), which comprises the cathodic hydrogen evolution reaction (hydrogen evolution reaction (HER); $2e^-$ transfer) and the anodic oxygen evolution reaction (oxygen evolution reaction (OER); $4e^-$ transfer), provides an effective pathway for large-scale production of green H_2[3]. However, the sluggish kinetics and high overpotentials of both reactions require efficient electrocatalysts to reduce energy consumption[4,5]. Noble-metal-based catalysts exhibit excellent performance but suffer from scarcity and high cost[6], limiting their large-scale utilization in EWS[7-9]. Meanwhile, non-noble metal catalysts have been widely explored, but they face challenges such as low conductivity, limited active sites, poor stability[10,11], and difficulty in catalyzing both HER and OER simultaneously.

Polyoxometalates (POMs), as defined by Herrmann *et al.*[12], are a class of molecular cluster compounds composed of early transition metals, such as tungsten (W), molybdenum (Mo), and vanadium (V), in high oxidation states [Figure 1], and have attracted increasing attention because of their tunable molecular architectures, abundant redox-active sites, excellent proton/electron transport capabilities, and high chemical stability[13-18]. These features make POMs inherently suitable for EWS, as their metal-oxygen clusters can act as multi-electron reservoirs to facilitate charge transfer and intermediate conversion[19,20]. However, the inferior activity of pristine POMs suffers from low electrical conductivity and severe agglomeration during EWS, which substantially suppress their catalytic performance[21-23]. To overcome these drawbacks, multifunctional modification strategies, including hybridization with conductive carriers (carbon-based substrates, metallic compounds, metal nanoparticles, *etc.*) and structural regulation (heteroatom doping, interface engineering), have been extensively adopted to reinforce the aqueous stability of POM anionic clusters, while simultaneously boosting electron transport efficiency and exposing sufficient accessible active sites[24-28]. Accordingly, POM-based EWS catalysts are regarded as highly promising candidates for efficient, durable, and low-cost water-splitting catalysis.

The development of POM-based EWS catalysts can be traced back to 1985, when Keita and Nadjo first reported the HER activity of POMs[12]; subsequent investigations have further validated their considerable potential in EWS systems. Benefiting from tunable molecular structures, reversible redox properties and well-defined active centers, POM-based catalysts have been extensively explored for performance optimization. For example, Feng *et al.*[29] constructed a "proton shuttle" by encapsulating Pt-POM in single-walled carbon nanotubes (SWCNT), significantly accelerating HER kinetics; Bibi *et al.*[30] developed a hybrid Anderson-type POMs that exhibits strong bifunctional catalytic performance, with overpotentials of 80 mV for the HER and 111 mV for the OER at a current density of 10 mA cm^{-2}. These studies demonstrate that noble metals with high intrinsic activity can be incorporated into POM skeletons at the atomic level with ultralow loading, thereby maximizing atom utilization and catalytic efficiency. Meanwhile, different categories of POMs display distinct catalytic preferences toward HER and OER. For instance, Keggin-type POMs with compact cluster structures are favorable for the HER owing to their superior proton adsorption capabilities, whereas Wells-Dawson-type POMs with larger frameworks exhibited high OER activity through multi-metal synergy[31,32]. Nevertheless, despite these significant advances, existing reviews lack a systematic

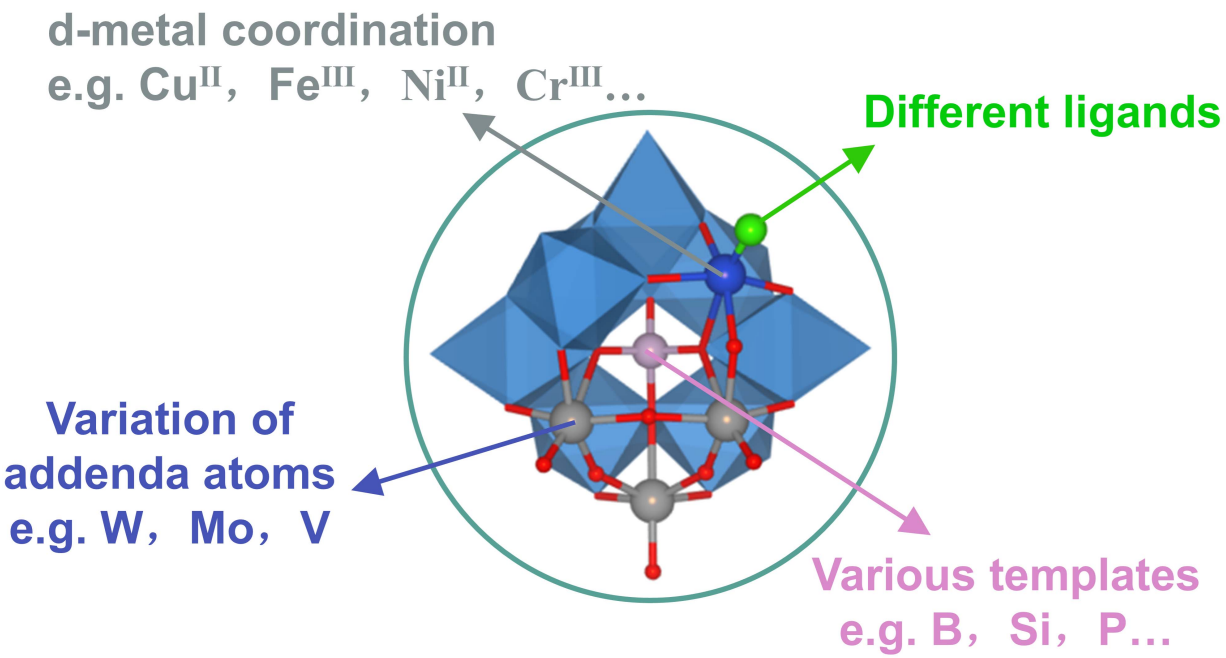

Figure 1. Schematic illustration of the structural features of Keggin-type POMs (Reproduced with permission from[12]. Copyright 2015, Royal Society of Chemistry).

analysis of how structural differences among POMs modulate HER/OER selectivity and overall bifunctional electrocatalytic performance.

To date, a large number of review articles have summarized the advances in POM-based electrocatalysis. Most existing works either introduce the versatile applications of POMs in various energy fields or discuss their catalytic performance for HER and OER separately, while few papers systematically compare the structural features of typical POM families and clarify the inherent correlation between POMs architectures and their catalytic selectivity toward different half-reactions. In addition, comprehensive discussions on structural modulation strategies, structure-dependent reaction pathways and practical challenges of POM-based electrocatalysts for water splitting are still lacking. To fill this research gap, this review focuses on the structural specificity of POMs and their derivatives, aiming to elaborate the intrinsic link between classical POM architectures—including Keggin, Wells-Dawson, Anderson structures—and their catalytic functions. We systematically summarize multidimensional modification strategies for POMs, illustrate how diverse structures regulate electronic states and catalytic pathways, and analyze current bottlenecks as well as feasible solutions. This work is expected to provide valuable theoretical guidance for the rational design and development of high-performance POM-based catalysts for EWS.

REACTION MECHANISM OF POM-BASED MATERIALS TOWARD EWS

The superior EWS catalytic performance of heterostructured POM-based materials originates from their unique multifunctional structural and electronic advantages[33-35]. As electron-deficient polyanionic clusters, POMs act as reversible electron reservoirs and charge regulators, which can continuously capture and redistribute interfacial electrons during electrocatalytic reactions, thereby tuning the electronic state of active centers and diminishing the kinetic barriers of both HER and OER. In particular, the strong interfacial electronic coupling between POMs and supporting components effectively modulates the adsorption strength of key water-splitting intermediates (i.e., H*, OH*, and OOH*), avoiding excessive or insufficient intermediate adsorption that commonly occurs in single-component catalysts[36,37]. Meanwhile, the

multi-metallic active centers and tunable lattice oxygen species of POMs provide abundant intrinsic catalytic sites, while heterointerfaces formed within the composites further expose accessible surface sites and accelerate mass and electron transport[38]. Such synergistic electronic modulation and structural optimization endow POM-based heterostructures with bifunctional catalytic capability, enabling efficient and stable overall water splitting (OWS) over a broad electrochemical window.

OER mechanism and POM structural preference

OER is a sluggish $4e^-/4H^+$ transfer reaction with high kinetic barriers, and its catalytic mechanism varies with electrolyte pH[39-41]. Yan *et al*.[42] reported that in alkaline media, hydroxide ions (OH^-) participate in the formation of reaction intermediates following the pathway of M-OH → M-O → M-OOH → O_2 [Figure 2A], whereas water molecules are directly oxidized under acidic conditions. For POM-based hybrid electrocatalysts, the inherent topological structures of POM components and strong interfacial electronic coupling between POMs and supporting substrates jointly regulate the entire OER catalytic pathway, including intermediate adsorption and conversion[43,44]. POMs with open extended frameworks and abundant polymetallic active sites (Wells-Dawson, Anderson, *etc*.) exhibit superior structural suitability for OER in composite systems[45]. Their large cluster configurations not only accommodate the multi-step electron transfer of the four-electron OER process, but also work synergistically with the adjacent substrate phase to optimize the adsorption strength of key intermediates (*O, *OH, *OOH) and promote efficient O-O bond coupling[46]. Specifically, Wells-Dawson-type POMs (e.g., $[P_2Mo_{18}O_{62}]^{6-}$) are composed of two Keggin-derived subunits connected by bridging oxygen atoms[47]. When integrated with metal oxides, carbon materials, or metal-organic frameworks (MOFs) to form hybrids, the unique dual-subunit structure strengthens intermetallic synergistic effects at the heterointerface, redistributes interfacial electrons, and further reduces the energy barrier of the rate-limiting O-O bond formation step. Meanwhile, the open skeleton of such POMs exposes more accessible active sites in hybrid systems, avoiding the aggregation of individual POM clusters and maintaining stable adsorption and conversion of OER intermediates. The corresponding OER equations under acidic and alkaline conditions are given in:

$$2H_2O \rightarrow O_2 + 4H^+ + 4e^- \text{ (acidity)} \quad (1)$$

$$4OH^- \rightarrow O_2 + 2H_2O + 4e^- \text{ (alkalinity)} \quad (2)$$

HER mechanism and POM structural preference

HER is a typical $2e^-/2H^+$ reduction reaction via Volmer-Heyrovsky or Volmer-Tafel mechanisms[48]. Ahmad *et al*.[49] proposed that in acidic electrolytes, H^+ undergoes direct cathodic reduction, whereas water dissociation acts as the rate-determining step in alkaline media [Figure 2B]. In POM-based hybrid systems, the compact cluster skeletons and strong proton adsorption capability of specific POMs (Keggin, Silverton, *etc*.) endow the composites with natural structural advantages for the HER[50]. Unlike pristine POMs, the combination of POM clusters and conductive substrates forms continuous charge-transfer channels throughout the hybrid material. The compact molecular configurations of Keggin-type POMs guarantee favorable proton adsorption and fast charge transfer kinetics at the interface. A representative Keggin-type POM ($[PW_{12}O_{40}]^{3-}$) consists of a central $\{PO_4\}$ tetrahedron encapsulated by twelve $\{MO_6\}$ octahedra[51]. Such dense architectures exhibit excellent redox reversibility. When anchored on metal oxides or carbon-based supports, intense electronic coupling between the two components modulates the d-band center of active sites, optimizes the adsorption free energy of adsorbed hydrogen (*H) intermediates following the Sabatier principle, and effectively accelerates the conversion of adsorbed protons into H_2 products. Additionally, POMs serve as "electron sponges" in hybrid systems, reversibly capturing and releasing electrons to supplement charge carriers and thereby further improving overall HER efficiency. The HER pathways under different pH conditions are summarized as:

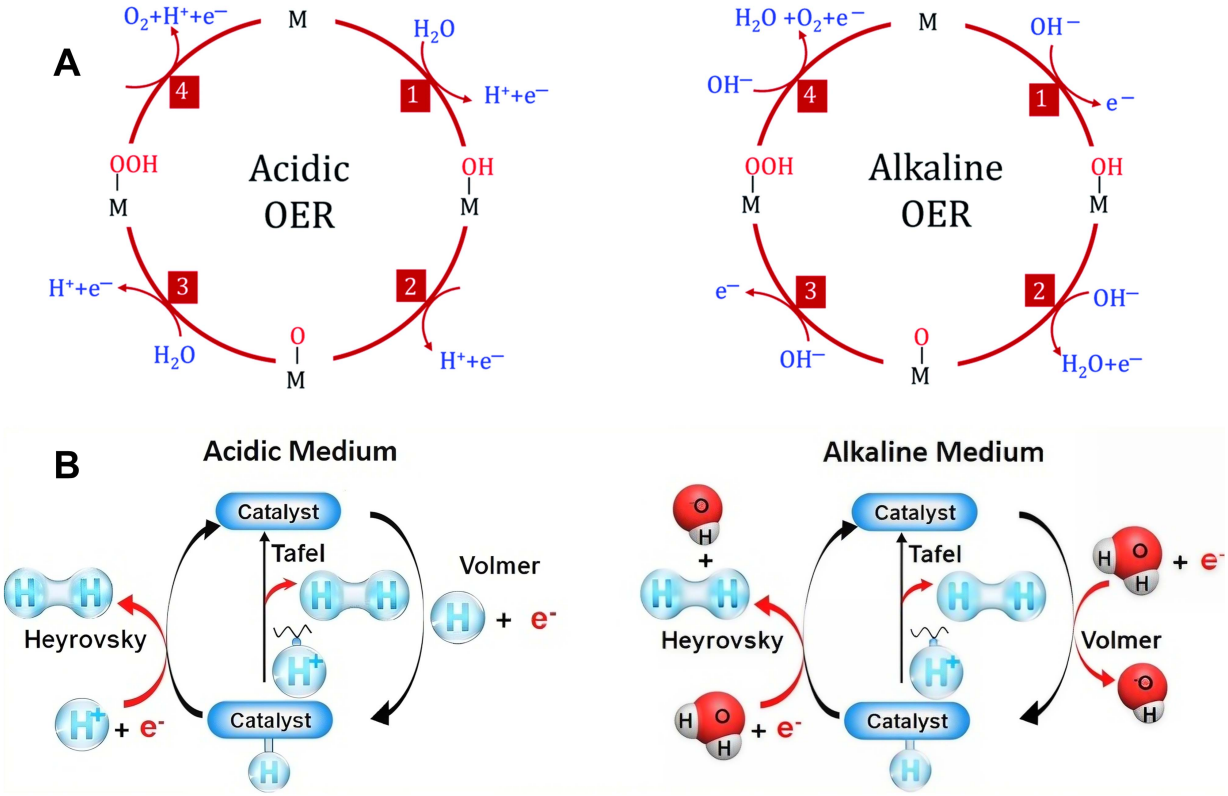

Figure 2. (A) Schematic illustration of feasible OER pathways in acidic and alkaline media (Reproduced with permission from[42]. Copyright 2020, Royal Society of Chemistry). (B) Schematic diagram of potential HER routes in acidic and alkaline media (Reproduced with permission from[49]. Copyright 2025, Wiley-VCH GmbH).

$$2H^+ + 2e^- \rightarrow H_2 \text{ (acidity)} \quad (3)$$

$$2H_2O + 2e^- \rightarrow H_2 + 2OH^- \text{ (alkalinity)} \quad (4)$$

STRUCTURAL SPECIFICITY OF POMS AND THEIR CATALYTIC ORIENTATION IN EWS

Keggin-type POMs

Keggin-type POMs with the general formula $[XM_{12}O_{40}]^{n-}$ are the most well-known and versatile POM archetype, featuring a central tetrahedral $\{XO_4\}$ heteroatom template (e.g., P, Si, B) encapsulated by 12 edge- and corner-sharing $\{MO_6\}$ octahedra built from addenda metals (e.g., W, Mo, V)[52]. As illustrated in Figure 3, such compact and highly symmetric topology provides numerous opportunities for structural modification[53-56]. Adjusting central heteroatoms and addendum metals can regulate cluster charge state, structural stability and redox properties; modifying surface ligands optimizes electrolyte solubility and intermediate adsorption behavior; doping with transition metals (Cu^{2+}, Fe^{3+}, Ni^{2+}) creates additional catalytic active sites[57,58]. Benefiting from flexible compositional tuning, favorable proton transport and abundant reversible redox sites, Keggin-type POMs are ideal candidates for high-efficiency HER, OER and bifunctional OWS electrocatalysis.

Wells-Dawson-type POMs

Wells-Dawson-type POMs are a prominent POM archetype with the general formula $[X_2M_{18-n}Y_nO_{62}]^{n-}$ (X = P, As, Si; M = Mo, W; Y = V, Cr, Co; *n* = 1-3), formed by two fused trilacunary Keggin fragments[59]. Their rich structural tunability, via central templates, addenda metals, substituted heteroatoms, surface ligands, and counter-cations, enables precise modulation of electronic properties and active sites, making them highly

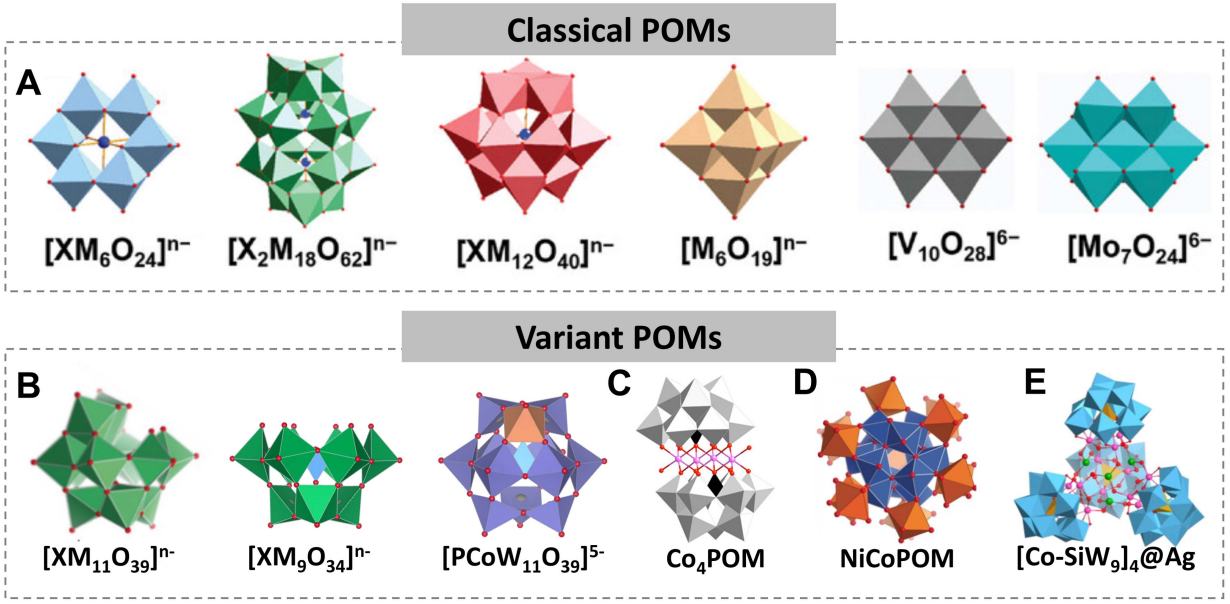

Figure 3. (A) Overview of common POM archetypes (Reproduced with permission from[52]. Copyright 2024, Wiley-VCH GmbH). (B) Schematic structure of lacunary POMs (Reproduced with permission from[53]. Copyright 2019, Wiley-VCH Verlag GmbH & Co. KGaA, Weinheim). (C) The molecular structure of the polyanions Co_4-Dawson-Wells (Reproduced with permission from[54]. Copyright 2012, American Chemical Society). (D) Dexter-Silverton polyoxometalate microcrystals (Reproduced with permission from[55]. Copyright 2017, Wiley-VCH Verlag GmbH & Co. KGaA, Weinheim). (E) POM-templated closed Ag clusters (Reproduced with permission from[56]. Copyright 2025, Wiley-VCH GmbH).

promising for OWS. Their structures can be tailored to simultaneously catalyze HER and OER through optimized proton/electron transfer and intermediate adsorption[60-62].

Anderson-type POMs

Anderson-type POMs, whose general formula is $[XM_6O_{24}]^{n-}$ ($2 \leq n \leq 8$, M denotes an addenda atom and X a central heteroatom), belong to the fundamental topological frameworks of the POM family[63] and possess a unique planar hexagonal structure distinct from the aforementioned POM frameworks. Their disc-like skeleton and high structural symmetry endow them with excellent electronic conductivity and abundant redox-active sites[64,65]. For OWS applications, tuning the central heteroatom, addenda metal atoms, or modifying the surface with organic ligands enables precise optimization of the electronic structure and active-site environment[66-68]. These modifications regulate the adsorption/desorption behavior of HER and OER intermediates, accelerate charge-transfer kinetics, and enable efficient and stable bifunctional electrocatalytic performance in EWS.

Other POM structures

In addition to the aforementioned Keggin, Anderson, and Wells-Dawson, the POM family also includes numerous other classical structural archetypes, including Lindqvist, Waugh, and Silverton clusters derived from Dawson skeletons[69,70], as well as distinctive structures such as lacunary, sandwich-type, and wheel-shaped POMs. Lindqvist POMs feature cage-like hexanuclear metal-oxo clusters with high symmetry and simple structural configurations[71-73]; Waugh POMs possess nonanuclear metal-oxo frameworks with unique three-dimensional pore channels[74,75]; Silverton POMs adopt cage architectures containing twelve coordinating heteroatoms, whose central cavities can accommodate bulky heteroatoms[76-78]. Moreover, lacunary POMs (e.g., mono-lacunary and tri-lacunary Keggin/Dawson species) serve as versatile building blocks, which can assemble with metal cations and organic chelates to construct various sandwich-type, extended and wheel-shaped POM clusters.

MODIFICATION STRATEGIES OF POMS

According to the distinctive structural features and catalytic properties of various POM families described above, this section systematically summarizes the research progress of POMs and POM-derived composite catalysts supported on diverse substrates for electrochemical water splitting. By analyzing the catalytic mechanisms of POMs in different reaction systems, the superior performances of POM-based electrocatalysts toward the HER and OER are comprehensively evaluated. Despite these merits, pristine POMs still suffer from intrinsically low electrical conductivity, susceptibility to aggregation, and insufficient structural stability during long-term electrocatalysis, which greatly limit their practical water-splitting efficiency. Under these circumstances, the rational introduction of suitable supporting substrates is essential to modulate the electronic structure, disperse POM active sites, and improve the overall electrode conductivity. Among various matrix materials, carbon-based supports have emerged as the most versatile and effective candidates for the modification and functionalization of POMs, because their unique conductive and structural characteristics can fundamentally remedy the shortcomings of pristine POMs and further boost the interfacial charge transfer and synergistic electrocatalysis of heterostructured POMs.

Carbon-based POMs

Carbon materials are widely adopted as ideal confined substrates and conductive carriers for POMs, owing to their rich structural diversity and electrical conductivities of 10^{2}-10^{6} S·cm^{-1}, thereby greatly accelerating electron transfer during EWS. Typical 2D carbon materials including graphene and g-C_3N_4[79] can anchor POMs via covalent linkage or intercalation confinement. Meanwhile, 3D carbon materials including carbon nanotubes (CNTs)[80] and microporous carbon[81] can be integrated with POMs through spatial encapsulation and surface immobilization. Nevertheless, carbon supports tend to undergo structural corrosion under long-term high-potential oxidation conditions, which inevitably compromises long-term catalytic activity. Heteroatom doping of carbon frameworks has therefore been developed to optimize surface electronic configurations and internal charge distributions, thereby markedly enhancing the long-term operational stability of POMs composites[82].

Graphene oxide

Graphene oxide (GO) possesses outstanding electrical conductivity, a wide electrochemical potential window, and abundant surface binding sites, and serves as an excellent substrate for immobilizing POM species[83]. For example, Li *et al.*[84] used $H_3PMo_{12}O_{40}$-PPy/reduced graphene oxide (rGO) as sacrificial precursors to synthesize Mo_2C encapsulated in N/P-codoped carbon (NPC) on N/P-codoped reduced graphene oxide (NPrGO), denoted Mo_2C@NPC/NPrGO [Figure 4A]. Transmission electron microscopy (TEM) showed that PMo_{12} was evenly distributed on rGO [Figure 4B]. High-resolution TEM (HRTEM) images also showed the unique porous structure of the as-obtained material, where 2-5 nm Mo_2C nanoparticles were densely dispersed on rGO nanosheets [Figure 4C]. The carbon coating successfully prevented the aggregation and excessive growth of Mo_2C NPs. Furthermore, electrochemical tests in 0.5 M H_2SO_4 (three-electrode system, 100 mV s^{-1} indicated that Mo_2C@NPC/NPrGO exhibited an onset overpotential of 0 mV and a low overpotential of ~34 mV at 10 mA cm^{-2}, superior to commercial Pt/C (40 mV) [Figure 4D]. These results demonstrated that rGO greatly facilitated the even dispersion of Mo_2C NPs and PMo_{12} clusters.

Carbon nanotubes

CNTs serve as typical one-dimensional conductive substrates, possessing a large specific surface area, outstanding electrical and thermal conductivity, and excellent mechanical stability. These merits make CNTs ideal hosts for POMs encapsulation and ensure fast multi-electron transfer throughout catalytic processes[85]. Quirós-Díez *et al.*[86] successfully fabricated the hybrid material 1@CNT by immersing carbon nanotubes in polar solvents to induce the assembly of anionic $[V_{10}O_{28}]^{6-}$ together with Na^{+} and

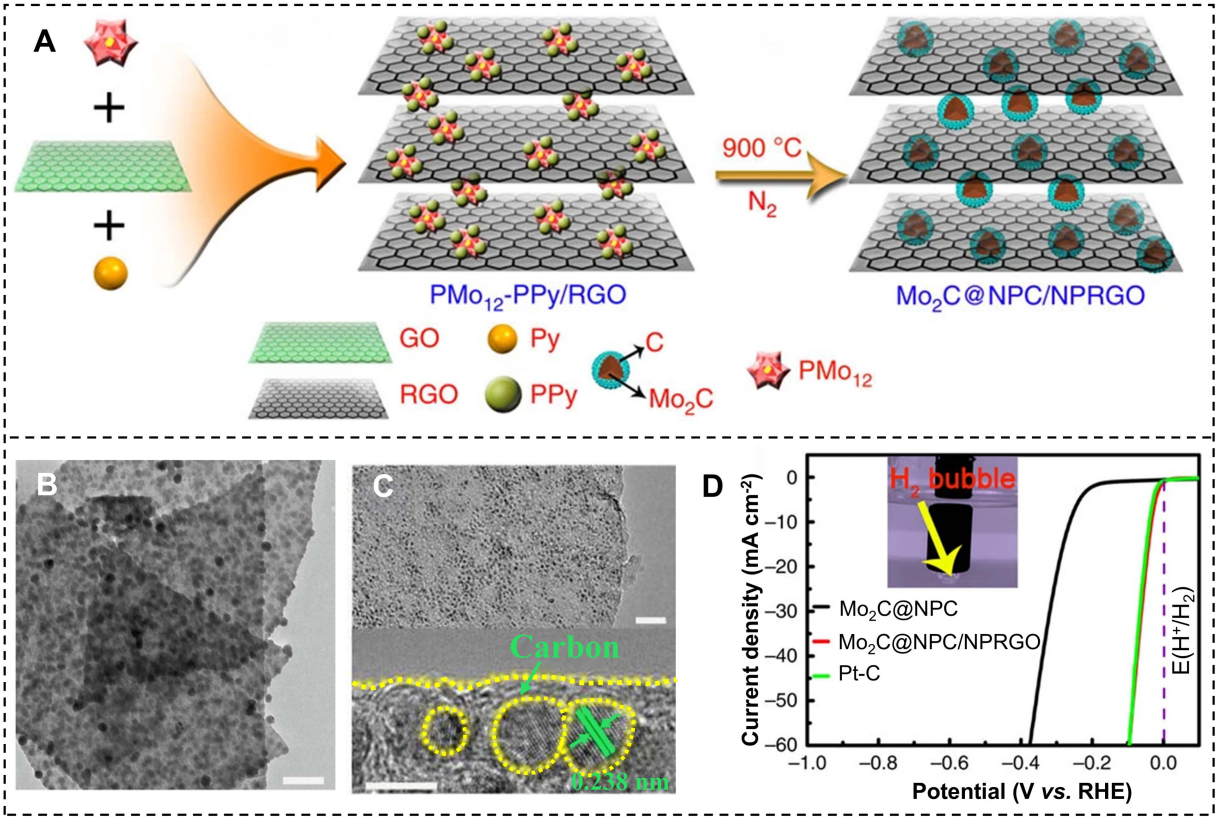

Figure 4. (A) Preparation of PMo_{12}-PPy/rGO and Mo_2C@NPC/NPrGO through an eco-friendly one-pot redox relay reaction. (B) TEM image of PMo_{12}-PPy/rGO, and (C) HRTEM image of Mo_2C@NPC/NPrGO. (D) Polarization curves of Mo_2C@NPC, Mo_2C@ NPC/NPrGO and Pt-C for the HER. (Inset: H_2 bubble generation on the Mo_2C@NPC/NPrGO surface). (A-D) Reproduced with permission from[84]. Copyright 2016, Springer Nature.

tris(hydroxymethyl)aminomethane ($TRIS^+$) cations on nanotube surfaces [Figure 5A]. HRTEM images confirmed that the carbon nanotubes were modified with $[V_{10}O_{28}]^{6-}$, Na^+ and $TRIS^+$ both internally and externally [Figure 5B]. The amorphous structure of the as-obtained material provided it with a large specific surface area and high electrochemical activity. Electrochemical tests in acidic media revealed that 1@CNT delivered excellent HER performance with an onset potential of -0.07 V [Figure 5C], approaching the performance of the commercial Pt/C benchmark. For OER, 1@CNT also exhibited a low onset potential (1.45 V) and overpotential (0.34 V) at 10 mA cm^{-2} [Figure 5D], which outperformed state-of-the-art Ir/C and IrO_2/C measured under identical acidic conditions. Combined with the anodic oxidation reaction (AOR) performance and corresponding reaction pathways depicted in Figure 5E, the results demonstrated that the $[V_{10}O_{28}]^{6-}$ moieties on 1@CNT acted as proton sponges to accelerate the OER process. This study identified regulation of crystal interactions through assembly engineering and modulation of counterion electrochemical properties as key strategies for constructing high-performance POM-based electrocatalysts for both HER and OER.

Porous carbon

Porous carbon materials are promising supports for POM-based electrocatalysts, featuring a high specific surface area and a 3D interconnected pore structure, excellent conductivity and tunable framework properties[87,88]. For example, Huang *et al.*[89] synthesized WS_2/Co_1S@N/S-codoped porous carbon nanocomposite via a one-step vulcanization-carbonization strategy, using phosphotungstic acid ($H_3PW_{12}O_{40}$)-encapsulated ZF-67 as precursors [Figure 6A]. Scanning electron microscopy (SEM) and TEM revealed that the High-temperature carbonization of ZIF-67 generated a 3D porous carbon framework

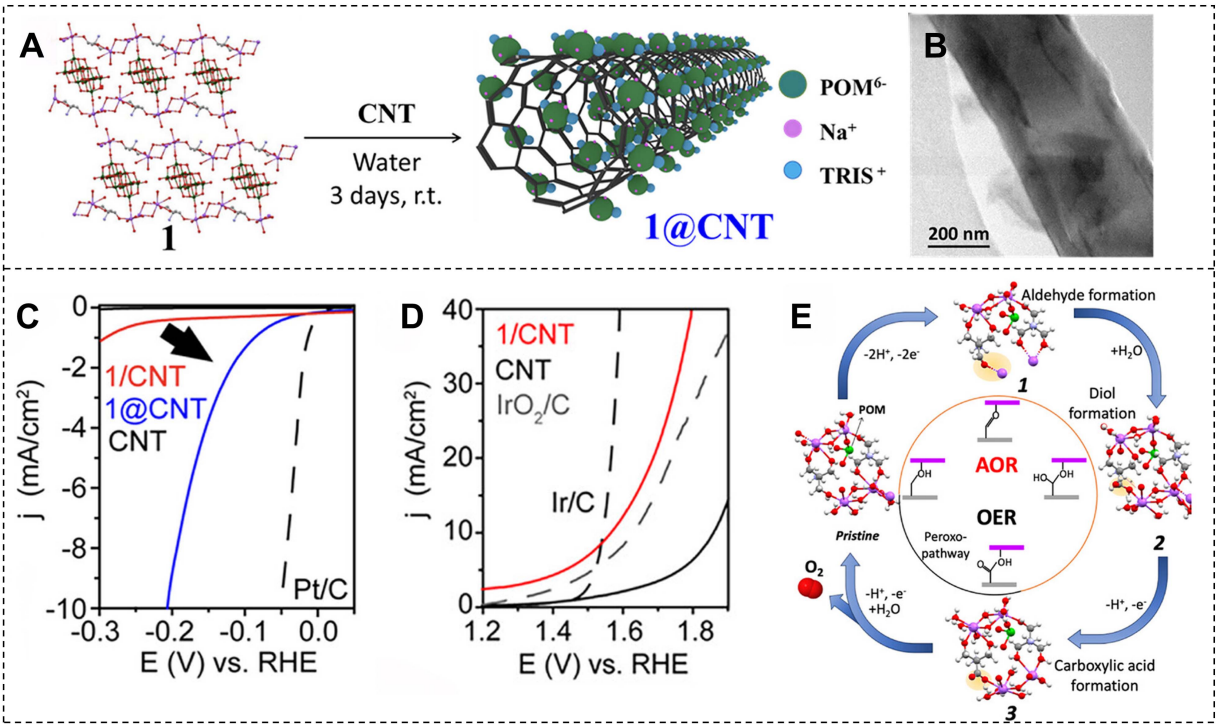

Figure 5. (A) Scheme illustration of the assembly process of $[V_{10}O_{28}]^{6-}$, Na^+ and $TRIS^+$ to form 1@CNT. (B) HRTEM image of 1@CNT acquired at 200 kV. (C) Linear sweep voltammetry (LSV) curves of 1/CNT (red), 1@CNT (blue), CNT (black), and commercial Pt/C benchmark catalyst for the HER. (D) Comparison of the OER catalytic performance of 1/CNT (red) and bare CNT (black), with Ir/C (black dashed line) and IrO_2/C as reference electrocatalysts. (E) Proposed mechanism for EWS over compound 1, involving an OER process coupled with the AOR. (A-E) Reproduced with permission from[86]. Copyright 2025, Wiley-VCH GmbH.

containing mesopores ranging from 1-50 nm, providing a confined space to inhibit aggregation of 5-10 nm metal sulfide particles during thermal treatment [Figure 6B and C]. Meanwhile, N/S co-doping enhanced the electron cloud density of the carbon matrix to promote charge transfer. Electrochemical measurements demonstrated that the as-obtained composite delivered remarkable HER and OER activities. It achieved a HER overpotential of 250 mV in 0.5 M H_2SO_4 [Figure 6D] and an OER overpotential of 365 mV at 10 mA cm^{-2} in 1 M KOH [Figure 6E]. Mechanistic studies revealed that the superior catalytic activity stemmed from the uniform distribution of $Co_{1-x}S$ and WS_2 nanoparticles within the heteroatom-doped carbon framework. Specifically, WS_2 derived from $[PW_{12}O_{40}]^{3-}$ served as an active component for the HER, which significantly increased the density of active sites in the composite. In addition, Cao *et al.*[90] synthesized Ni_3N and Co nanoparticles supported on N-doped porous carbon (PW-NiCo-NC) by calcination, based on the favorable matching of pore and cavity dimensions between ZIF-8/67 and Keggin-type $H_3PW_{12}O_{40}$ [Figure 6F]. A TEM image confirmed that PW-NiCo-NC displayed a typical hollow cage morphology with obvious inner cavities [Figure 6G], in which the active nanoparticles were uniformly dispersed on the carbon cage shells. Electrochemical measurements were carried out using the device shown in Figure 6H. The catalyst achieved superior HER activity in 1 M KOH, with an overpotential of 211 mV and a Tafel slope of 106.9 mV dec^{-1} at 10 mA cm^{-2}. Remarkably, the excellent HER activity was mainly attributed to the combined merits of POMs and porous carbon, in which POMs served as efficient active centers to regulate interfacial electron distribution and enrich catalytic sites, and the porous hollow carbon structure enlarged the active surface area and shortened ion/electron diffusion pathways, thereby fundamentally optimizing the reaction kinetics of EWS.

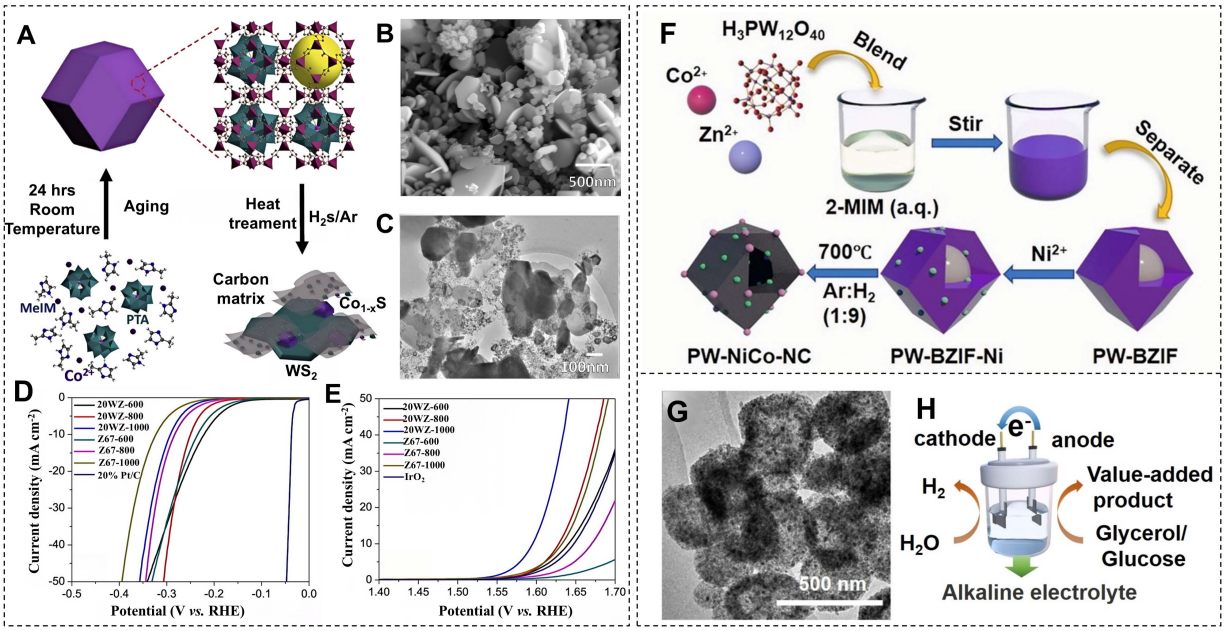

Figure 6. (A) Schematic illustration of the synthesis of $WS_2/Co_{1-x}S$@N/S-codoped carbon nanocomposite. (B) SEM and (C) TEM images of 20WZ-1000, (D) HER polarization curves of benchmark catalyst 20% Pt/C, and (E) OER polarization curves of benchmark catalysts IrO_2, carbonized/sulfurized W20@Z67 and ZIF-67 under 600, 800 and 1,000 °C. (A-E) Reproduced with permission from[89]. Copyright 2020, Elsevier Ltd. (F) Synthetic scheme, and (G)TEM image of PW-NiCo-NC. (H) Schematic illustration of the EWS device. (F-H) Reproduced with permission from[90]. Copyright 2023, Wiley-VCH GmbH.

Metal-based POMs

Transition metal compounds have garnered widespread research attention for EWS owing to their natural abundance, low cost, and tailorable catalytic activity[91]. Among them, metal oxides[92], metal sulfides[93], metal phosphides[94], and metal carbides[95] have been widely explored as EWS catalytic materials. These compounds possess abundant surface active sites and adjustable electronic structures, enabling strong interfacial interactions with POMs. As efficient electron reservoirs, POMs can spontaneously modulate interfacial charge distribution, thereby optimizing the adsorption-desorption processes of catalytic intermediates and reinforcing the synergistic effect between heterogeneous phases.

Metal oxides

Metal oxides have emerged as an important class of electrocatalytic materials, benefiting from their robust structural durability, distinctive electronic structures, and adjustable valence state characteristics[96]. However, inherent limitations such as insufficient catalytic activity and ambiguous active site identification persist[97]. Integrating metal oxides with POMs has emerged as an effective strategy to construct rapid charge transfer interfaces and augment active site density[98-100]. Cui *et al.*[101] synthesized nanoflower-like POM-$Fe_{0.2}Ni_{0.8}Co_2O_4$ heterostructures on nickel foam (NF) via an *in-situ* hydrothermal strategy [Figure 7A and B]. The introduced tri-vanadium-substituted Keggin-type POM clusters (PMo_9V_3) functioned as electron sponges with abundant reversible redox centers, while the heterogeneous interface between POM and spinel $Fe_{0.2}Ni_{0.8}Co_2O_4$ induced strong electronic modulation and optimized interfacial electron distribution. This unique synergy created numerous undercoordinated active sites, accelerated proton-coupled electron transfer, and facilitated the migration as well as adsorption/desorption of reaction intermediates in the EWS process. Meanwhile, the combination of POM and $Fe_{0.2}Ni_{0.8}Co_2O_4$ effectively increased the surface roughness and electrochemical active surface area (ECSA) of the composite[52], further exposing accessible active sites and alleviating particle aggregation. Benefiting from these favorable characteristics, the POM-$Fe_{0.2}Ni_{0.8}Co_2O_4$/NF catalyst delivers exceptional bifunctional catalytic performance. At a current density of 10 mA cm^{-2}, it required overpotentials

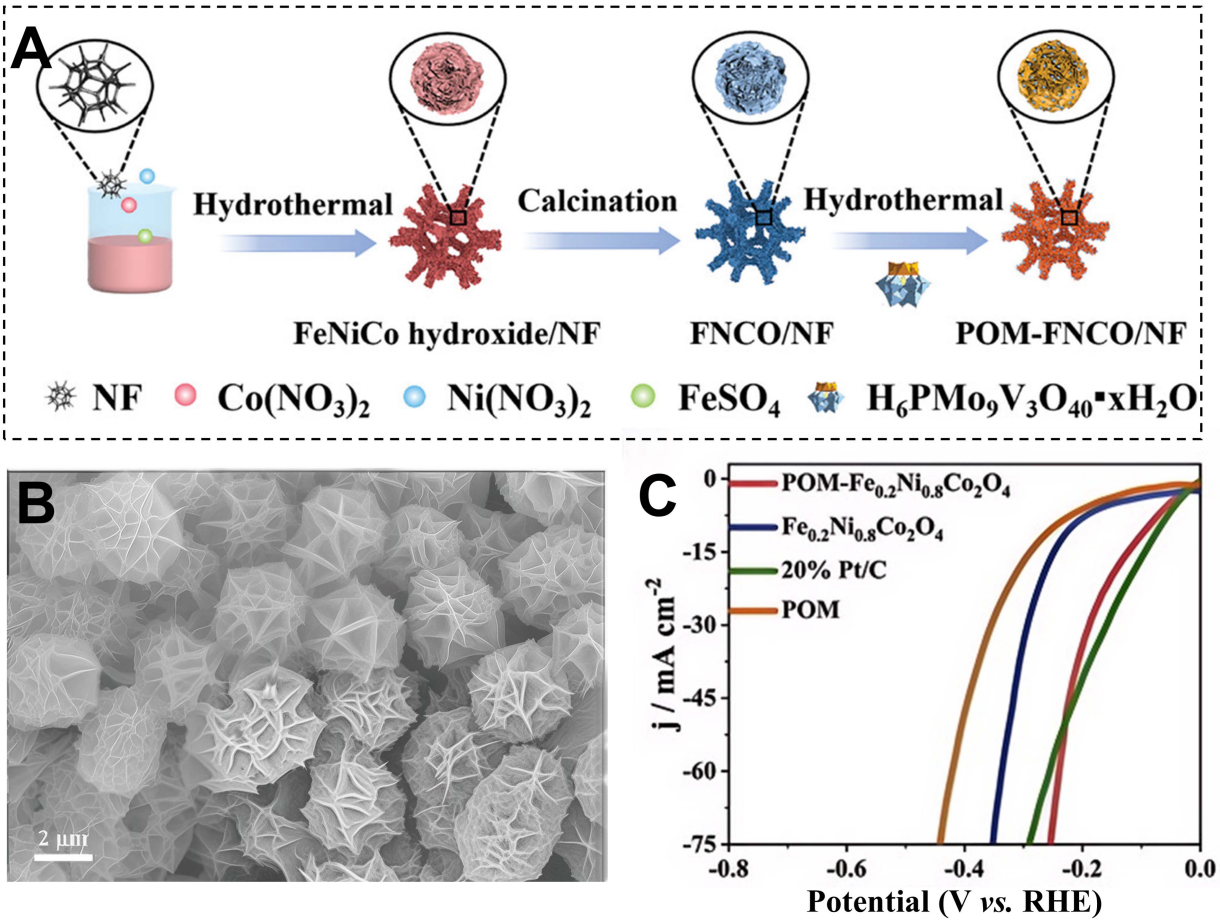

Figure 7. (A) Schematic illustration, (B) SEM image of POM-FNCO/NF. (C) HER LSV curves of POM-$Fe_{0.2}Ni_{0.8}Co_2O$/NF and other reference samples. (A-C) Reproduced with permission from[101]. Copyright 2024, Wiley-VCH GmbH.

of only 89 mV for the HER and 259 mV for the OER, respectively [Figure 7C], outperforming the single-component POM and $Fe_{0.2}Ni_{0.8}Co_2O_4$ catalysts as well as commercial noble-metal benchmarks. When integrated into a two-electrode OWS system, the fabricated electrolyzer required a low cell voltage of 1.58 V to attain a current density of 10 mA cm^{-2}, demonstrating its great potential for practical EWS applications.

Metal sulfides

Metal sulfides suffer from inherently strong metal-sulfur bonding, which limits OER kinetics and hinders their widespread application in EWS[102]. However, incorporating POMs units into metal sulfides has proven effective in modulating their physicochemical properties, introducing abundant transition metal active sites and tailoring charge distribution. Gautam *et al.*[103] further fabricated a POM-coated Zn-Co sulfide nanowire heterostructure (POM@ZnCoS/NF) on NF via a facile two-step hydrothermal method [Figure 8A]. A TEM image revealed that POM (PW_{12}) nanoparticles were firmly anchored on the surfaces of ZnCoS nanowires [Figure 8B]. This coating roughened the nanowire surfaces, increased the specific surface area, and enhanced electrocatalytic activity. When tested using the setup shown in Figure 8C, the POM@ZnCoS/NF electrode delivered better catalytic performance than commercial Pt/C (for HER) and RuO_2 (for OER) in 1 M KOH. For HER, POM@ZnCoS/NF achieved overpotentials of 170 and 337 mV to reach 10 and 40 mA cm^{-2}, respectively. LSV measurements were adopted to evaluate its OER activity, and the catalyst only required overpotentials of 200 and 300 mV at 20 and 50 mA cm^{-2}. Furthermore, Guillen-Soler *et al.*[104] constructed a POM/Pd/MoS_2 heterostructure by integrating molybdenum disulfide (MoS_2) flakes, palladium (Pd) nanoparticles, and cobalt-doped POM (Co-POM) [Figure 8D]. The hybrid featured an interwoven fibrous

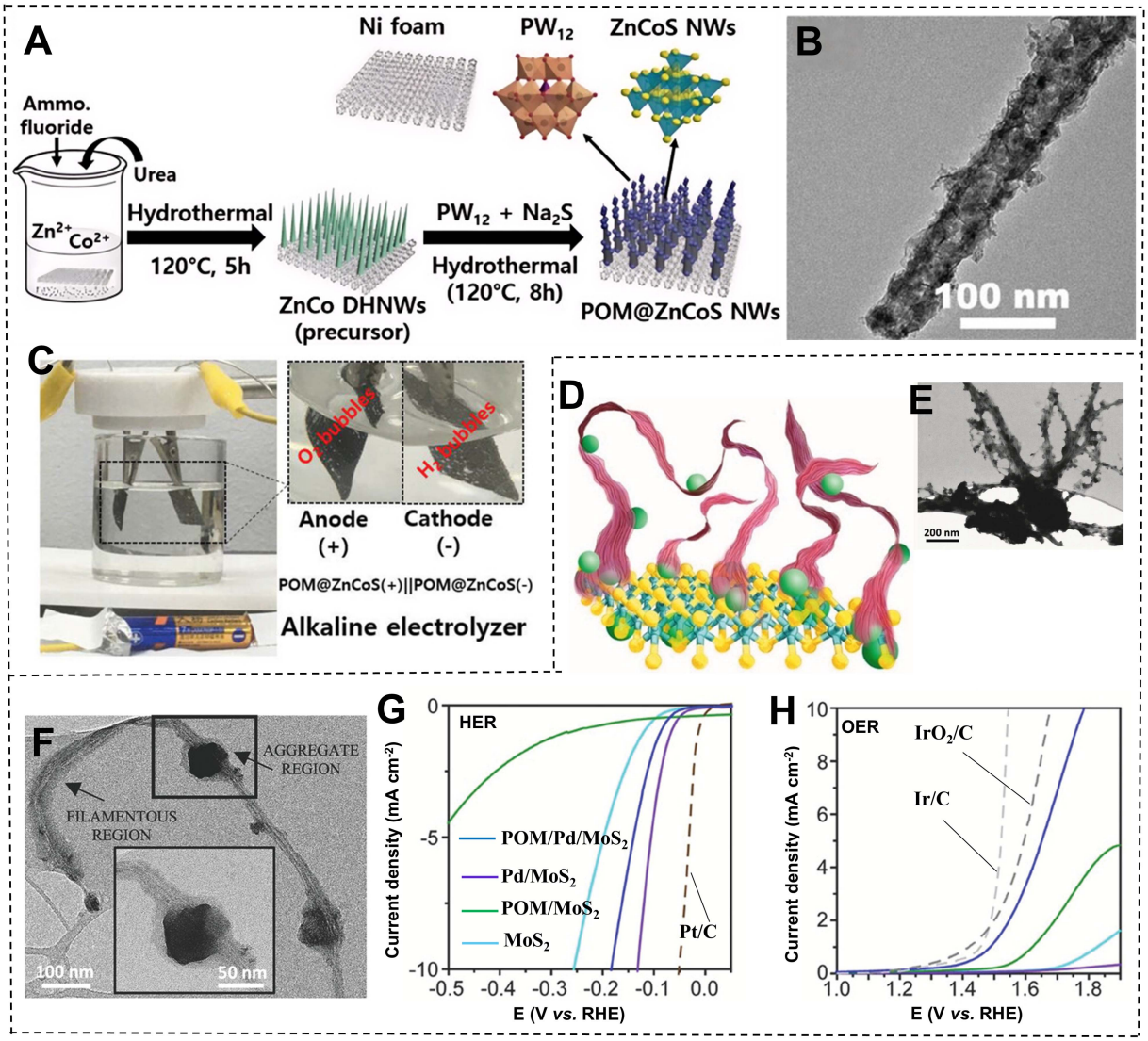

Figure 8. (A) Synthetic route for POM@ZnCoS NWs, (B) TEM image of POM@ZnCoS NWs, (C) Generation of O_2 and H_2 bubbles on the anode and cathode of the POM@ZnCoS/NF electrode at a cell voltage of 1.5 V. (A-C) Reproduced with permission from[103]. Copyright 2021, Wiley-VCH GmbH. (D) Schematic illustration, (E) Representative field-emission SEM image, (F) HRTEM image of the POM/Pd/MoS_2 hybrid composite. (G) HER and (H) OER polarization curves after ohmic drop correction for the prepared catalysts. (D-H) Reproduced with permission from[104]. Copyright 2023, Wiley-VCH GmbH.

morphology that substantially increased the specific surface area and exposed more active sites [Figure 8E and F]. Benefiting from the synergistic effects among the three components, the heterostructure exhibited HER and OER activity comparable to commercial noble-metal catalysts. Electrochemical tests in 0.1 M NaOH and 0.5 M H_2SO_4 demonstrate onset potentials of 0.10 V (HER) and 1.45 V (OER). Correspondingly, low overpotentials of 0.08 and 0.25 V were obtained at 10 mA cm^{-2} for the HER and OER, respectively [Figure 8G and H]. Moreover, the catalyst maintained robust long-term durability, sustaining stable electrocatalytic output over 8 h of continuous operation. These studies confirmed that combining POMs with metal sulfides provided complementary advantages. The unique structural properties of POMs and the distinctive catalytic properties of metal sulfides worked together to greatly boost the OWS performance of the as-obtained bifunctional electrocatalysts.

Metal phosphides

Metal phosphides exhibit high intrinsic HER activity because phosphorus atoms favor proton adsorption, whereas metal atoms facilitate the adsorption/desorption of hydrogen intermediates[105]. Additionally, they facilitate rapid electron transfer and enhanced OER kinetics[106]. However, transition metal phosphides are often fabricated into working electrodes using binders, which may cause mechanical detachment of active species or chemical instability[107,108]. Owing to the rich surface charge distribution of POMs, their integration with metal phosphides enables controllable formation of electrostatic interactions, hydrogen bonds, or covalent bonds, thereby alleviating the aforementioned issues. Integrating POMs with metal phosphides therefore offers a viable and efficient strategy for the rational design of electrocatalysts with superior activity, long-term stability, and potential for scalable application. Jiao *et al.*[109] assembled lamellar precursors from PMo_{12} clusters and egg white through hydrogen bonds. Subsequent high-temperature phosphorization treatment enabled the *in situ* formation of N/P/S-tripledoped carbon layers, transforming the precursors into porous sheet-structured MoP@NPSC composites [Figure 9A]. HRTEM images showed that well-crystallized MoP nanoflakes were encapsulated and linked by thin carbon layers, and the distinct lattice spacings of 0.210 and 0.278 nm corresponded to the (101) and (100) crystal planes of MoP, confirming the intimate interfacial contact between diverse crystalline facets [Figure 9B and C]. Owing to its distinctive porous nanosheet architecture, the MoP@NPSC composite delivered markedly improved HER catalytic performance. It achieved a low overpotential of 50 mV at 10 mA cm^{-2}, which was much lower than that of pristine MoP (89 mV) [Figure 9D]. The results confirmed that POM-derived metal phosphides enabled homogeneous distribution of metal sites and formed intimate interfaces, thereby regulating electronic structures and hydrogen adsorption properties. Zhao *et al.*[110] constructed a densely porous phosphide composite (MoP/MoNiP@NPC-800) via high-temperature pyrolysis using $[Ni(2,2'\text{-bipy})_3][Mo_6O_{19}]$ (Ni-POM) and $NaH_2PO_2{\cdot}H_2O$ as precursors [Figure 9E]. The composite presented a honeycomb-shaped porous aggregate morphology, and TEM characterization revealed that MoP and MoNiP nanoparticles were encapsulated within graphitic carbon layers [Figure 9F]. Owing to the synergistic effect of dual MoP/MoNiP active sites and the stabilizing effect of NPC, the catalyst delivered a low overpotential of 50.4 mV at 10 mA cm^{-2} in 1 M KOH [Figure 9G], which was lower than the values reported for most previous MoNi-based HER electrocatalysts. Moreover, electrochemical impedance spectroscopy (EIS) measurements revealed that MoP/MoNiP@NPC-800 exhibited a smaller Nyquist semicircle than the other four catalysts [Figure 9H]. A simplified equivalent circuit was adopted to fit the Nyquist plots. The minimum charge-transfer resistance (R_{ct}) of 5.88 Ω indicated the excellent electrical conductivity and fast interfacial charge transfer kinetics of MoP/MoNiP@NPC. This study further verified that the introduction of POM units could create additional active sites and thus improve the HER and OER performance of phosphide-based electrocatalysts.

Layered double hydroxides

Transition-metal-based layered double hydroxides (LDHs) exhibit outstanding bifunctional electrocatalytic activity for HER and OER in alkaline media, primarily due to their favorable nanoarray architectures[111,112]. However, inherent drawbacks such as poor electrical conductivity and limited accessible active sites restrict their further development[113]. Integrating POMs with LDHs has emerged as an effective strategy to address these limitations by constructing synergistic heterostructures. Wang *et al.*[114] reported an *in situ* anchoring approach to immobilize $[PCoW_{11}O_{39}]^{5-}$ (Co-POM) nanoparticles onto NiFe-LDH nanosheets via hydrothermal treatment, forming Co-POM@LDH composites [Figure 10A]. TEM and HRTEM lattice analyses confirmed the formation of three-dimensional heterostructures [Figure 10B and C]. Electrochemical tests revealed that Co-POM@LDH/NF delivered HER and OER overpotentials of 220 and 226 mV at 10 mA cm^{-2} in 1.0 M KOH, respectively [Figure 10D and E]. More notably, the two-electrode electrolyzer assembled with Co-POM@LDH/NF as both the anode and cathode required an ultralow cell voltage of 1.51 V to drive OWS at 10 mA cm^{-2} [Figure 10F]. This remarkable performance was attributed to the abundant Co-POM nanoparticles firmly anchored on LDH nanosheets, which formed heterostructures with

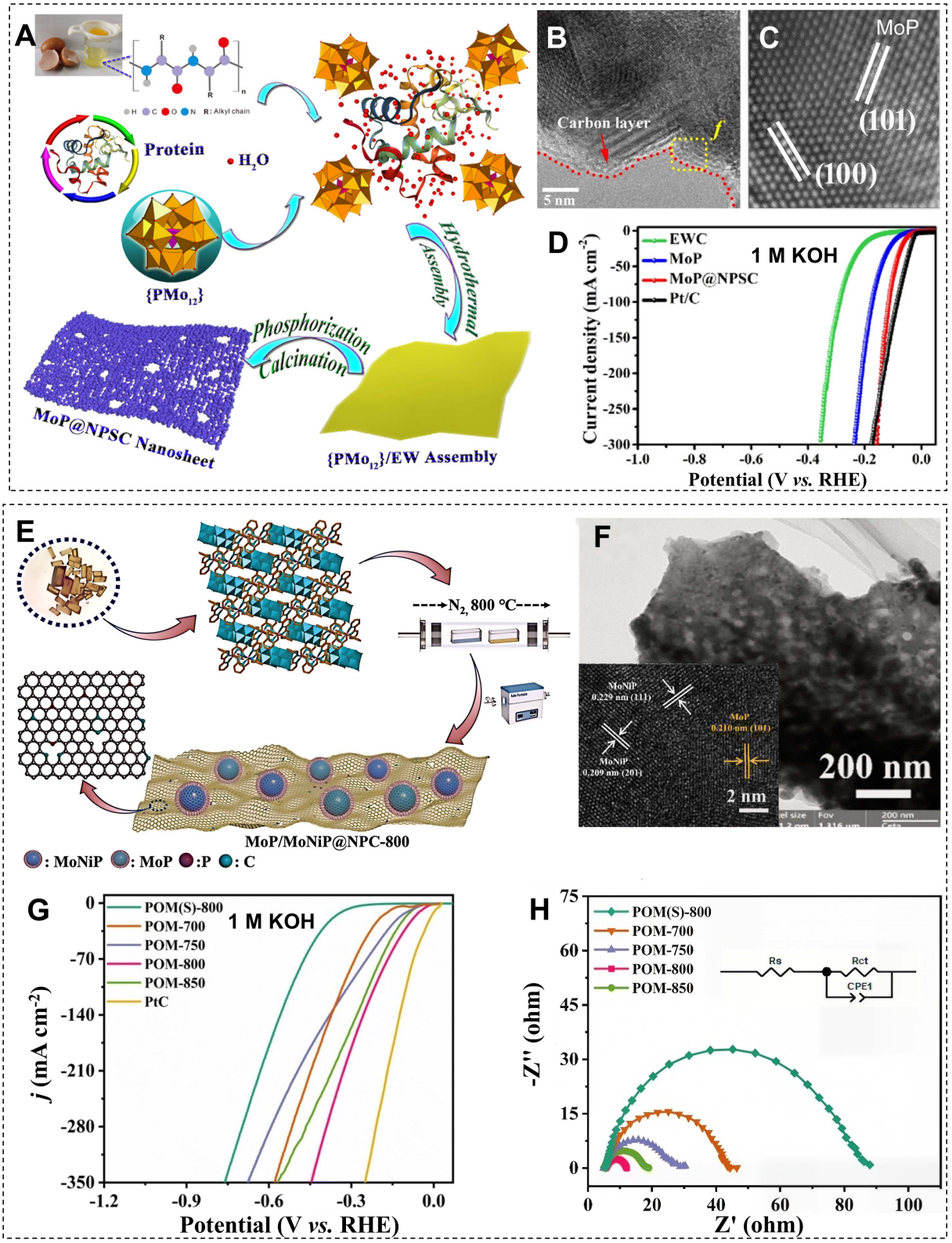

Figure 9. (A) Schematic of the formation mechanism for MoP@NPSC. (B and C) HRTEM images of MoP@NPSC. (D) HER polarization curves of bare EWC, MoP, MoP@NPSC, and Pt/C recorded in 1 M KOH at a scan rate of 5 mV s^{-1}. (A-D) Reproduced with permission from[109]. Copyright 2020, American Chemical Society. (E) Preparation route of the MoP/MoNiP@NPC-800 catalyst via pyrolysis treatment. (F) TEM image of MoP/MoNiP@NPC-800 (inset: corresponding HRTEM image). (G) HER polarization curves in 1 M KOH, (H) EIS Nyquist plots of five POM-derived catalysts tested in 1 M KOH (inset: corresponding equivalent circuit). (E-H) Reproduced with permission from[110]. Copyright 2024, Royal Society of Chemistry.

numerous active sites and large specific surface areas, thereby accelerating electron and mass transport. Furthermore, the introduced Co-POM component could offer abundant active species, including Co^{2+} ions and labile lattice oxygen species, to further boost catalytic reactions. Using a similar approach, Zhang *et al.*[115] synthesized phosphotungstic acid (PTA)-intercalated NiFe-LDH (NiFe-LDH-PTA) electrocatalysts on NF via a one-step hydrothermal method [Figure 10G]. SEM images revealed that NiFe-LDH-PTA presented a uniform and ultrathin cross-linked nanosheet structure without any agglomeration [Figure 10H]. Such structural features enabled NiFe-LDH-PTA to achieve the highest OER activity across all catalysts. Its overpotentials reached 220 ± 3, 267 ± 5, and 306 ± 8 mV at 100, 300, and 600 mA cm^{-2}, far superior to pristine NiFe-LDH (258, 332 and 411 mV) [Figure 10I]. Given its excellent OER performance, an anion-exchange membrane (AEM) electrolyzer using NiFe-LDH-PTA||Pt/C as the electrodes was assembled [Figure 10J], demonstrating great potential for industrial hydrogen generation. Collectively, these works proved that LDHs were ideal carriers for POMs in bifunctional HER/OER catalysis. Electron-rich POMs effectively adsorbed H^*, while electron-deficient LDHs activated H_2O/OH^- and facilitated O-O bond formation with the assistance of POMs. Additionally, LDHs promoted water dissociation and supplied sufficient H^* to accelerate H_2 desorption.

Metal nanoparticles

Composites of POMs and metal nanoparticles (MNPs) hold great promise for precisely tailoring charge distribution and engineering active sites, with POM clusters serving as core electronic modulators governing the electrocatalytic properties and reaction kinetics of the hybrid system[116,117]. Li *et al.*[118] synthesized Keggin-type $[PW_{12}O_{40}]^{3-}$ (PW_{12})/Ag/graphene composites using $Ag(H_3biim)_2$ as both a POM-binding ligand and Ag precursor [Figure 11A]. An HRTEM image revealed distinct lattice fringes with an interplanar spacing of 0.234 nm, which corresponded to the (111) crystal plane of face-centered cubic (fcc) silver (Ag) [Figure 11B]. The controlled release of Ag^+ from the $Ag(H_3biim)_2$ during N,N-dimethylformamide (DMF) reflux effectively suppressed nanoparticle agglomeration, and the presence of PW_{12} further promoted the uniform dispersion of Ag nanoparticles on graphene. LSV measurements demonstrated that the PW_{12}/Ag/graphene-a catalyst exhibited an overpotential of 540 mV at 10 mA cm^{-2}, surpassing pristine graphene, Ag/graphene, and PW_{12}/graphene counterparts [Figure 11C]. This remarkable OER activity stemmed from the synergistic interplay between PW_{12} and AgNPs, wherein Ag accelerated interfacial electron transfer, whereas the PW_{12} cluster functioned as a critical electronic regulator to refine the electronic configuration of Ag and promote H_2O activation. Moreover, the multi-oxo bridging skeleton of PW_{12} offered abundant surface oxygen sites that facilitated O-O bond formation, thus further boosting OER kinetics. Notably, although MNP-decorated POMs were mainly explored for OER catalysis, the intrinsic redox behavior and flexible electronic structure of POMs drove the conversion of MNPs from electron-rich to electron-deficient states, ultimately enhancing their intrinsic catalytic activity. Meanwhile, the graphene support ensured fast electron transport and structural robustness, collectively contributing to the improved electrocatalytic performance.

MOF-based POMs

MOFs have become ideal host materials for constructing POM-MOF hybrids (POMOFs) owing to their inherent merits including tunable porous structures, large specific surface areas and customizable functional sites[119,120]. The strong host-guest interaction between POM clusters and MOF skeletons effectively regulates electronic distribution and accelerates electron transfer, which optimizes the redox behavior of POMs and produces a pronounced greater-than-additive synergistic effect in EWS. A series of typical POM@MOF electrocatalysts have been investigated for the HER and OER. For instance, Zhang *et al.*[121] encapsulated Keggin-type PMo_{12} clusters into Co-based MOF-74 via a one-step solvothermal strategy to fabricate PMo_{12}@MOF-74 composites [Figure 12A]. The composite exhibited a distinct nanorod morphology, as observed in Figure 12B. The MoC@CoO catalyst derived from PMo_{12}@MOF-74 showed remarkable HER performance [Figure 12C]. EIS further confirmed its rapid charge transfer capability [Figure 12D]. In

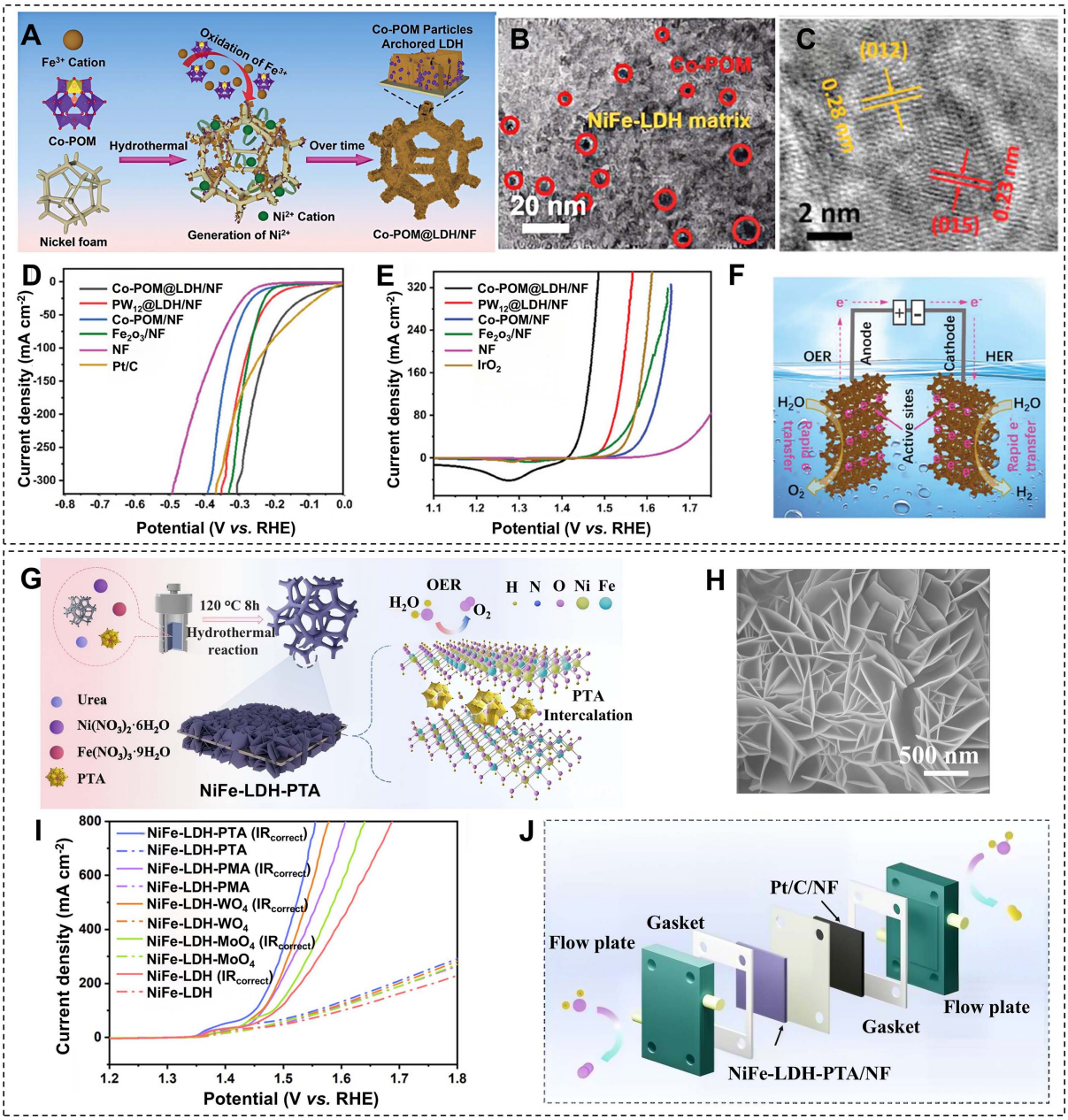

Figure 10. (A) Synthetic schematic of Co-POM@LDH/NF. (B) TEM and (C) HRTEM images of Co-POM@LDH/NF. (D) HER polarization curves of Co-POM@LDH/NF, PW_{12}@LDH/NF, Co-POM/NF, Fe_2O_3/NF, bare NF and Pt/C at 5 mV s^{-1}. (E) OER polarization curves of Co-POM@LDH/NF, PW_{12}@LDH/NF, Co-POM/NF, Fe_2O_3/NF, bare NF and IrO_2 at 5 mV s^{-1}. (F) Schematic configuration of a two-electrode electrolyzer using Co-POM@LDH/NF. (A-F) Reproduced with permission from[114]. Copyright 2023, Wiley-VCH GmbH. (G) Fabrication schematic of NiFe-LDH-PTA grown on NF. (H) SEM image of NiFe-LDH-PTA. (I) OER polarization curves with and without iR compensation at a scan rate of 2 mV s^{-1}. (J) Schematic illustration of the AEM electrolyzer configuration. (G-J) Reproduced with permission from[115]. Copyright 2025, American Chemical Society.

addition, Zeb *et al.*[122] adopted a scalable hydrothermal strategy to synthesize Mo-CuS/NiS/NF on NF using POM-MOF composites as precursors [Figure 12E]. SEM and TEM images verified the successful synthesis of the material, which formed vertically aligned and regularly arranged nanorods on the substrate surface [Figure 12F]. Uniform Mo doping derived from the $NiMo_6$ precursor efficiently tuned the electronic configuration of the composite. Benefiting from the cooperative interactions generated at bimetallic sulfide heterojunctions, the material provided numerous exposed catalytic sites and drastically lowered the kinetic barrier toward hydrogen evolution. When tested at 10 mA cm^{-2}, the electrocatalyst achieved overpotentials of

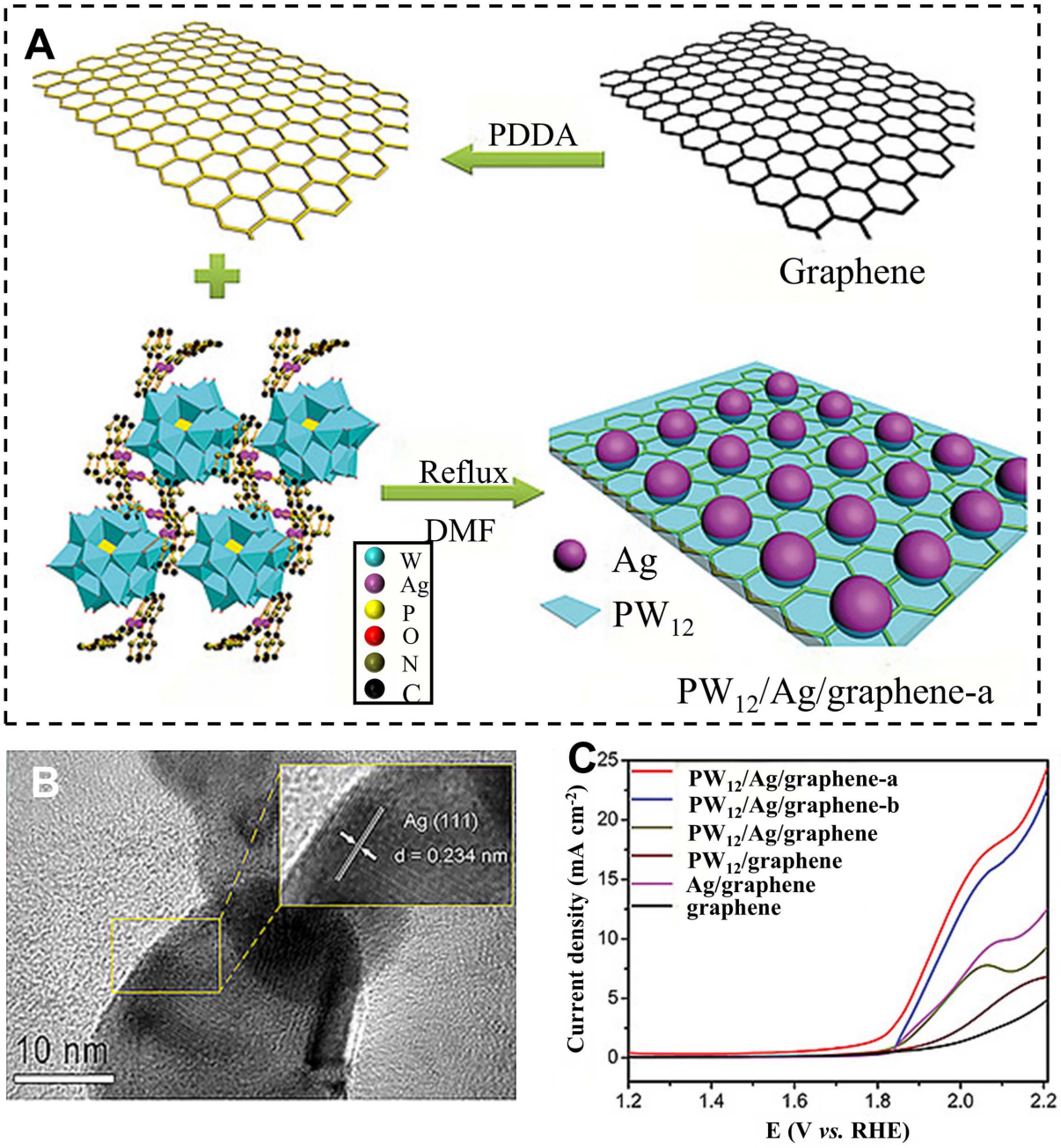

Figure 11. (A) Proposed growth mechanism, (B) HRTEM image of PW_{12}/Ag/graphene-a. (C) LSV curves obtained in 0.1 mol L^{-1} phosphate-buffered saline (PBS; pH = 7.0) using a glassy carbon electrode (GCE) modified with a series of graphene-based hybrid catalysts. (A-C) Reproduced with permission from[118]. Copyright 2019, Wiley-VCH Verlag GmbH & Co. KGaA, Weinheim.

78, 95 and 111 mV in alkaline medium, artificial seawater, and natural seawater, respectively, which surpassed the catalytic activity of NF loaded with commercial 20% Pt/C [Figure 12G]. Density functional theory (DFT) simulations uncovered the alkaline HER pathway over Mo-CuS/NiS/NF and validated that the catalytic reaction followed the Volmer-Heyrovsky route. As visualized in Figure 12H, the complete catalytic mechanism of HER on Mo-CuS/NiS/NF under alkaline conditions is illustrated, demonstrating that Mo-doped active centers and CuS/NiS heterointerfaces cooperated to facilitate successive reaction steps: water capture, H-O bond cleavage, and the subsequent formation and release of H_2.

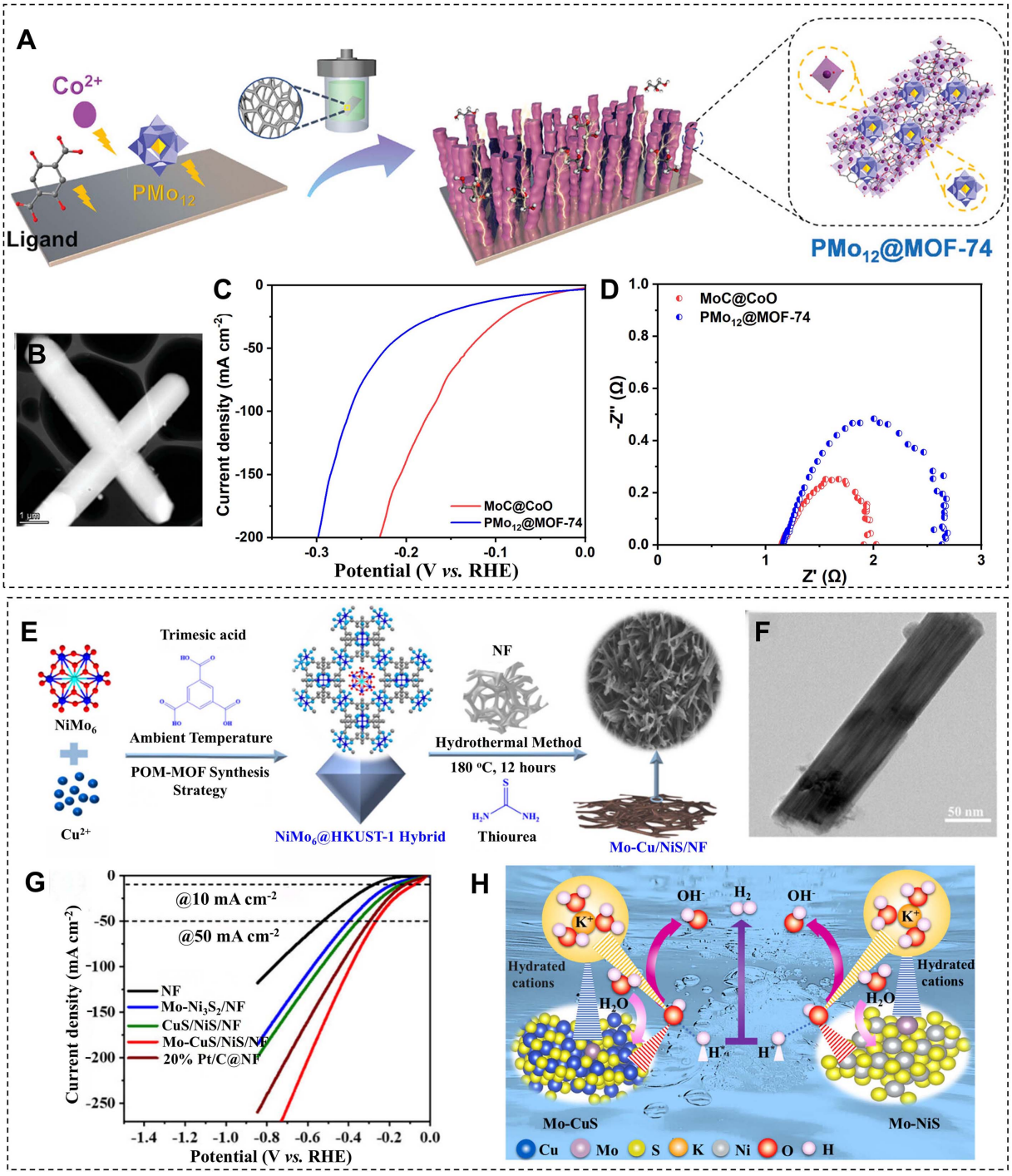

Figure 12. (A) Synthetic schematic diagram, (B) high-angle annular dark-field scanning transmission electron microscopy (HAADF-STEM) image and corresponding elemental distribution mapping of PMo_{12}@MOF-74. (C) LSV curves, (D) Nyquist impedance curves of MoC@CoO and PMo_{12}@MOF-74 for the HER. (A-D) Reproduced with permission from[121]. Copyright 2025, Wiley-VCH GmbH. (E) Synthesis scheme, (F) HRTEM image of Mo-CuS/NiS/NF. (G) LSV curves of the synthesized catalysts compared with 20% Pt/C@NF *vs.* reversible hydrogen electrode (RHE) for the HER. (H) Illustration of the mechanism of alkaline HER on Mo-CuS/NiS/NF. (E-H) Reproduced with permission from[122]. Copyright 2025, American Chemical Society.

These studies demonstrated that the outstanding electrocatalytic activity of POMOF hybrid composites stemmed from their porous MOF frameworks. Such structural backbones supplied numerous accessible active sites and facilitated rapid mass transport kinetics. Intense electronic coupling at the heterogeneous interfaces between POM clusters and MOF substrates reshaped the electron distribution of active centers and

Table 1. Summary of electrocatalytic HER performance for POM-based materials

Support	POM	Overpotential at 10 mA cm^{-2} (η_{10}) (mV *vs.* RHE)	Tafel slope (mV dec^{-1})	Electrolyte	Cycling stability (h)	Morphology	Synthesis method	Ref.
Ni-Mo_2C@N, P co-doped carbon	$NiMo_6O_{24}$	η_{500} = 268 η_{500} = 295	59 64	0.5 M H_2SO_4 1 M KOH	12	Nanoparticles uniformly distributed on carbon	Supramolecular-confinement pyrolysis strategy	[123]
Co_9S_8@MoS_2	PMo_{12}	230	84	1 M KOH	48	Assembled nanosheets	One-pot calcination	[124]
CoP-WP/rGO	Co_8W_{18}	130	54	0.5 M H_2SO_4	30	Nanoparticles distributed on the thin graphene layer	Hydrothermal treatment, air calcination, and phosphorization	[125]
C_3N_4	Mo_7O_{24}	164 95	33 62.1	0.5 M H_2SO_4 1 M KOH	48	Cylinders	Hydrothermal, high-temperature vulcanization	[126]
Ni MOF	$[MoO_4]^{2-}$	35	52.5	1 M KOH	120	Nanosheet array	Hydrothermal, chemical vapor deposition	[127]
Ag-H_2biim	SiW_{12} P_2W_{18}	112 91	77 65	0.5 M H_2SO_4	10	Homogeneous fluffy and spongy surfaces	Hydrothermal	[128]
HMCS	$Co_4(PW_9)_2$	25 105	36 43	0.5 M H_2SO_4 1 M KOH	60	Hollow mesoporous spheres	High-temperature vulcanization	[129]
MoS_2@CC	Co_2Mo_{10}	120 153	64 71	1 M KOH 0.5 M H_2SO_4	24 25	Nanoflower	Hydrothermal	[130]
Zn/Co ZIF-L	PMo_{12}	80.6	128	1 M KOH	16	Hexagram-like porous structure	Self-assembly and high-temperature vulcanization	[131]
Ni@PTM	$[Mo_7O_{24}]^{6-}$	30.1	79.4	1 M KOH	100	Rough layer decorated with uniform nanoparticles	Electrodeposition	[132]
HMCS	PW_9	58 60	69 97	0.5 M H_2SO_4 1 M KOH	80	Hollow mesoporous carbon spheres	Hydrothermal	[133]

HMCS: Hollow mesoporous carbon spheres; CC: carbon cloth; PTM: porous titanium mesh; ZIF-L: leaf-like zeolitic imidazolate framework; HER: hydrogen evolution reaction; POM: polyoxometalate; RHE: reversible hydrogen electrode.

lowered the kinetic barrier of rate-limiting reaction steps. Meanwhile, boosted surface wettability accelerated electrolyte infiltration and the release of gaseous products. All these structural merits provide useful guidance for the rational fabrication and performance optimization of robust POMOF composite electrocatalysts toward efficient EWS.

COMPARISON OF DIFFERENT POM-BASED CATALYSTS IN EWS

Tables 1-3 systematically summarize the electrocatalytic performance of diverse POM-based hybrid composites for HER, OER, and OWS, respectively. Key parameters, including HER and OER overpotentials at 10 mA cm^{-2}, full water-splitting cell voltage, electrolyte type, cycling stability, catalyst morphology, and synthesis strategy, are compared. By correlating these performance indicators with POM molecular structures and corresponding support types, the analysis reveals the dominant effects of cluster topology, metal coordination environment, defect engineering, and interfacial electronic interaction on the electrocatalytic behavior. This comprehensive performance overview provides theoretical support for the rational structural design of highly efficient water-splitting electrocatalysts, and facilitates the practical evaluation of POM-based materials for industrial-scale EWS.

Table 2. Summary of electrocatalytic OER performance for POM-based materials

Support	POM	Overpotential at 10 mA cm^{-2} (η_{10}) (mV *vs.* RHE)	Tafel slope (mV dec^{-1})	Electrolyte	Cycling stability (h)	Morphology	Synthesis method	Ref.
$ZnFe_2O_4$	P_2Mo_{18}	η_{20} = 270	124.6	1 M KOH	20	Nanoplates	Hydrothermal	[134]
WS_2/WO_3@C	SiW_9	610	65	0.1 M KOH	8	Nanosheets decorated with particles and rod-like structures	Vulcanization	[135]
IF	$H_3PMo_{12}O_{40}$	282	45.5	1 M KOH	12	Nanoflowers	Facile etching	[136]
NiO-Ru/RuO_2	$[V_{10}O_{28}]^{6-}$	300	112	1 M KOH	5.6	Layered-like structure	Hydrothermal	[137]
PCN	$[Mo_7O_{24}]^{6-}$	340	67.4	0.1 M KOH	100	Single-atom	Pyrolysis	[138]
WS_2	Co_5W_{19}	297	55	1 M KOH	72	Willow catkin-like structure	Hydrothermal treatment and vulcanization	[139]
Mg_2Al-LDH	$[Co_4(H_2O)_2(PW_9O_{34})_2]^{10-}$	567	275	0.1 M sodium phosphate + 1 M $NaNO_3$	24	Hexagonal layered structures	Stirring	[140]
		464	87	0.1 M sodium borate + 1 M $NaNO_3$				
NH_2-MIL-101	Ni_4Mo_{12}	332.6	58	1 M KOH	6	Nanoparticles	Grinding	[141]
	Co_4Mo_{12}	352.6	54.8					
ZIF-67	PW_{12}	306	54	1 M KOH	15	Hollow structure	Chemical etching, cation exchange, and thermal annealing	[142]
C-Mn_2O_3	$[TiCoW_{11}O_{40}]^{7-}$	300	88	1 M KOH	100	Waxberry-like shape	Self-assembly	[143]

IF: Iron foam; PCN: polymeric carbon nitride; OER: oxygen evolution reaction; POM: polyoxometalate; RHE: reversible hydrogen electrode.

CONCLUSION AND OUTLOOK

This review systematically summarizes the core significance of state-of-the-art progress in POMs and their derivatives for EWS, with emphasis on their structural modulation strategies and the intrinsic relationship between their architectures and bifunctional electrocatalytic activity for water splitting. We comprehensively discuss the synthetic methods for POM composites with various supporting materials, including carbides, metallic compounds, and MOFs, as well as cutting-edge advances in structural construction and rational design of microscale active sites for POM derivatives. Meanwhile, the catalytic pathways and mechanisms of the HER and OER are also discussed in detail.

Nevertheless, despite encouraging progress achieved to date, numerous critical challenges remain to be addressed for POM-based catalytic materials. For instance, pristine POMs inherently suffer from low intrinsic electrical conductivity, facile dissolution and leaching in electrolytes, and insufficient long-term stability under harsh

Table 3. Summary of electrocatalytic OWS performance for POM-based materials

Support	POM	HER overpotential at 10 mA cm^{-2} (η_{10}) (mV *vs.* RHE)	OER overpotential at 10 mA cm^{-2} (η_{10}) (mV *vs.* RHE)	Overall water-splitting voltage (V) (j = 10 mA cm^{-2})	Electrolyte	Cyclic stability (h)	Morphology	Synthesis method	Ref.
NF	$H_6PV_3Mo_9O_{40}$	89	259	1.58	1 M KOH	48	Nanoflower	Hydrothermal	[101]
NiFe-LDH	$PCoW_{11}$	70	193	1.51	1 M KOH	48	Nanoparticles anchored on nanosheets	Hydrothermal	[114]
WO_2-W	$PW_{11}Ir$ and $PW_{11}Pt$	41	250	1.46	1 M KOH	100	Hollow sphere	Organic encapsulation and calcination	[144]
ZnFe LDH	P_2Mo_{18}	η_{20} = 275	η_{20} = 330	1.54	1 M KOH	40	Porous nano-clusters	Hydrothermal	[145]
$Ni(OH)_2$	$H_5PV_2Mo_{10}O_{40}$	32	243	1.50	1 M KOH	60	Porous ultrathin nanosheets	Hydrothermal	[146]
$Ni_3S_2/NiMo_2$	$H_3O_{40}PW_{12}{\cdot}xH_2O$	η_{100} = 275	η_{100} = 338	1.53	1 M KOH	20	Flower-like nanosheets	Hydrothermal	[147]
Ni-MOF	$[P_2W_{18}O_{62}]^{6-}$	68	107	1.51	1 M KOH	24	Nanoparticles anchored on hexagonal prisms	Ball-milling	[148]
RuO_2	$SiW_{10}O_{36}$	46	142	1.42	0.5M H_2SO_4	100	Core-shell	Electrodeposition	[149]

NF: Nickel foam; OER: oxygen evolution reaction; POM: polyoxometalate; RHE: reversible hydrogen electrode; HER: hydrogen evolution reaction;OWS: overall water splitting.

reaction conditions. Meanwhile, the mode of hybridization between POMs and supporting substrates also exerts a substantial influence on the resulting catalytic performance. Consequently, precise manipulation of POM-based composite architectures remains difficult in most studies, leading to poor catalyst uniformity and impeding their scalable industrial application. Furthermore, the interfacial interaction mechanisms between POM clusters and supports remain poorly understood, and structurally analogous composites often display divergent catalytic behaviors, which severely hinder rational development in this field. In addition, the formation pathways of inorganic catalysts derived from POM precursors have rarely been explored, resulting in poor predictability of the morphology, structure, and composition of the final derivatives.

Various *in situ* characterization techniques, including Fourier-transform infrared spectroscopy (FTIR), X-ray diffraction (XRD), and SEM/TEM, and other relevant testing tools, can not only uncover the microstructural features of POM-based catalysts but also track the structural evolution of POMs during catalytic processes and provide guidance for structural optimization. These techniques help clarify the advantages of atomic-level regulation and uniform distribution of unique active sites in POM building units and supports, facilitating the construction of stable, efficient, and mechanistically well-understood electrocatalytic systems. However, such characterization methods are limited by sophisticated equipment, demanding operational requirements, and restricted experimental environments, which can impede the advancement of related materials. Accordingly, future research directions are proposed as follows.

(1) *In situ* X-ray absorption fine structure (XAFS) spectroscopy should be combined with DFT calculations to deepen fundamental mechanistic studies of POM-based composites, enabling precise identification of active sites, real-time monitoring of dynamic structural evolution throughout reactions, and quantitative analysis of synergistic interactions between POMs and supports.

(2) Multiple targeted structural tuning approaches, including accurate heteroatom incorporation, vacancy manipulation, and heterostructure construction, should be exploited to synergistically enhance charge-transport capacity and the stability of catalytic centers in POM-derived electrocatalysts for EWS, while fine-tuning the adsorption free energies of critical reactive intermediates.

(3) Data-driven tools such as machine learning should be introduced to establish intelligent frameworks for materials design. Using the extensive performance and structural data summarized in this review and related literature, these approaches can accelerate the screening of optimal POM configurations, suitable support combinations, and ideal synthetic parameters.

(4) Industrial water electrolysis applications require intensified investigations into the practical performance of POM-based catalysts in proton-exchange membrane (PEM) and AEM electrolyzers. By optimizing interfacial electron transport and membrane-electrode compatibility, durability and overall water-splitting efficiency should be systematically evaluated under high current densities and strongly acidic or alkaline conditions. A correlation framework linking half-cell performance to full electrolyzer device performance should be established to advance the real-world application of POM-derived electrocatalysts for large-scale clean hydrogen manufacturing.

In summary, POM-based electrocatalysts, with their abundant raw materials and flexible, precisely tunable structures, are expected to play an important role in renewable energy, biomedicine, and ecological restoration. This review provides a systematic overview of POM-based composite catalysts in EWS research, demonstrating that these materials represent promising candidates to support global carbon-neutrality goals and reduce dependence on fossil fuels. With a deeper understanding of structural regulation principles and catalytic reaction mechanisms of POMs, they are expected to become highly competitive electrocatalysts for EWS and play an important role in industrial catalysis.

DECLARATIONS

Acknowledgments

We gratefully acknowledge that all graphical fragments integrated into the Graphical Abstract were reproduced with formal copyright permissions granted by the corresponding publishers. Copyright attributions are listed as follows: Copyright © 2016, The Author(s) (Figure 1A used in POM-Graphene); Copyright © 2019 Wiley-VCH Verlag GmbH & Co. KGaA, Weinheim (Scheme 1 used in POM-AgNPs); Copyright © 2024, Royal Society of Chemistry (Visual Abstract used in POM-PdNPs); Copyright © 2021, American Chemical Society (Scheme 1 used in POM-AuNPs); Copyright © 2023, American Chemical Society (Figure 7 used in POM-PEI); Copyright © 2024, American Chemical Society (Figure 1C used in POM-MOF); Copyright © 2022, American Chemical Society (Scheme 1 used in POM-COF); Copyright © 2023 Wiley-VCH GmbH (Figure 1 used in POM-LDH); Copyright © 2023, American Chemical Society (Figure 1 used in POM-Metal Oxides); Copyright ©2023 The Authors. Advanced Sustainable Systems published by Wiley-VCH GmbH (Figure 3B used in POM-Metal Sulfides); Copyright © 2025 Wiley-VCH GmbH (Figure 1 used in POM-Carbon nanotubes); Copyright ©2025, American Chemical Society (Figure 1C used in POM-Carbon foam); Copyright © 2016 SIOC, CAS, Shanghai & Wiley-VCH Verlag GmbH & Co. KGaA, Weinheim (Figure 1 used in POM species for EWS).

Authors' contributions

Data sourcing, collection, and original draft writing: Wang, T.

Data sourcing: Wang, W.
Data analysis and interpretation: Ma, X.; Xuan, M.
Editing and supervision: Chen, G.; Labidi, A.
All authors participated in preparing the manuscript.

Availability of data and materials

Not applicable.

AI and AI-assisted tools statement

Not applicable.

Financial support and sponsorship

This work was supported by the National Natural Science Foundation of China (22578100), the Natural Science Foundation of Henan Province (252300421904), the Key Scientific Research Projects of Higher Education Institutions in Henan Province (26A610002, 25A610002), the High-level Talent Research Launch Fund of Henan University of Technology (2024BS050, 2023BS104), and the National Key Research and Development Program of China (2023YFB4203605).

Conflicts of interest

All authors declared that there are no conflicts of interest.

Ethical approval and consent to participate

Not applicable.

Consent for publication

Not applicable.

REFERENCES

1. Faizan, M.; Bibi, H.; Aamir, E.; Saeed, R.; Kiong, T. S.; Song, H. Efficient chromium-based transition metal nitrides catalysts for oxygen and hydrogen evolution reactions. *Renew. Sustain. Energy. Rev.* **2025**, *212*, 115385. DOI
2. Zhang, Y.; Liang, W.; Yao, S.; Zheng, Z.; Wang, C. Preparation and performance of Co-Mo nano metal oxide electrocatalyst for hydrogen production by electrolysis of water. *Fuel* **2026**, *404*, 136253. DOI
3. Sun, X.; Fu, Y.; Chen, R.; et al. $Fe^{II}Fe^{III}$-prussian blue modulated Fe-vacancies of NiFe-layered double hydroxide for oxygen evolution reaction with high stability. *Appl. Surf. Sci.* **2025**, *703*, 163399. DOI
4. Abbas, F.; Talib, S. H.; Mohamed, S.; Wei, Y. Thermodynamic stability, mechanistic evaluation, and electronic properties of polyoxoniobate-based SACs (TM@PONb): a promising multifunctional electrocatalyst for HER/OER/ORR. *J. Phys. Chem. C.* **2025**, *129*, 13203-18. DOI
5. Dong, X.; Fang, X.; Li, B.; et al. Solar energy storage in polyoxometalate for on-demand hydrogen transportation and evolution. *Adv. Mater.* **2025**, *38*, e19875. DOI
6. Wang, T.; Wang, W.; Zhu, Y.; Zhang, B. Electro-fenton degradation of rhodamine B with in-situ H_2O_2 generation by Au nanoparticles modified reduced graphene oxide. *J. Environ. Chem. Eng.* **2025**, *13*, 115685. DOI
7. Hanan, A.; Lakhan, M. N.; Awan, H. T. A.; Walvekar, R.; Azat, S.; Khalid, M. Advances in magnesium-based non-PGM electrocatalysts for efficient overall water splitting. *Int. J. Hydrogen. Energy.* **2026**, *203*, 153043. DOI
8. Yu, M.; Ye, Q.; Wang, F.; et al. Ternary metal NiRuPt partition synergistic relay promotes pH-universal hydrogen evolution. *Nano. Res.* **2026**, *19*, 94907879. DOI
9. Zhang, K.; Wang, K.; Chai, S.; et al. Engineering Ru-based electrocatalysts for efficient electrocatalytic water splitting. *Nano. Res.* **2025**, *18*, 94907369. DOI
10. Chen, J.; Li, Y. Preparation of lignin derived carbon encapsulating Molybdenum/Nickel bifunctional materials and their application in overall water splitting. *Chem. Eng. Sci.* **2025**, *310*, 121528. DOI
11. Chen, T.; Guo, Q.; Ye, J.; Jiang, Q.; Chai, N.; Yi, F. Metal-organic framework-derived bimetallic FeNi sulfide nanostructures for electrolysis of water and urea. *ACS. Appl. Nano. Mater.* **2025**, *8*, 2730-40. DOI

12. Herrmann, S.; Ritchie, C.; Streb, C. Polyoxometalate - conductive polymer composites for energy conversion, energy storage and nanostructured sensors. *Dalton. Trans.* **2015**, *44*, 7092-104. DOI PubMed
13. Zhang, L.; Xu, Q.; Xia, L.; et al. Asymmetrically tailored catalysts towards electrochemical energy conversion with non-precious materials. *Chem. Soc. Rev.* **2025**, *54*, 5108-45. DOI
14. Zhang, Y.; Li, R.; Wang, X.; et al. Surface active-site engineering of low-noble-metal-alloyed metallic glass catalyst for boosting water electrolysis. *Adv. Funct. Mater.* **2024**, *34*, 2410379. DOI
15. Nandy, A.; Murmu, G.; Rana, A.; Saha, S.; Banerjee, S. Sprayed microdroplets architect a polyoxometalate framework. *Angew. Chem. Int. Ed.* **2025**, *64*, e202424745. DOI PubMed
16. Shah, W. A.; Dai, X.; Zhai, X.; Zhao, Y.; Zhang, Y.; Li, S. Precise size-matching between guest polyoxometalates and host metal-organic frameworks enables enhanced photocatalytic water oxidation. *Commun. Chem.* **2025**, *9*, 29. DOI PubMed PMC
17. Xiong, L.; Liu, S.; Chen, W.; et al. Assembly of sandwich-type ruthenium-containing polyoxometalates for efficient construction of C-C bonds. *Chem. Commun.* **2026**, *62*, 7353-6. DOI
18. Zhang, T.; Guo, L.; Xie, W.; Hou, S.; Li, S.; Li, Y. Three-dimensionally ordered macro-mesoporous $ZrTiO_4$ supported polyoxometalate-ionic liquid hybrid for efficient biodiesel production from low-quality oils. *Appl. Surf. Sci.* **2026**, *730*, 165882. DOI
19. Cui, X. Special Issue: Research on polyoxometalate materials. *Molecules* **2023**, *28*, 4662. DOI PubMed PMC
20. Stamate, A.; Pavel, O. D.; Zavoianu, R.; Marcu, I. Highlights on the catalytic properties of polyoxometalate-intercalated layered double hydroxides: a review. *Catalysts* **2020**, *10*, 57. DOI
21. Abdollah Pour Aghdam Sharabiani, S. M. A.; Rezvani, M. A. Synthesis and characterization of new tri- titanum substituted Keggin-type polyoxometalate ($PW_9Ti_3O_{40}$) for enhanced photocatalytic water oxidation performance. *Inorg. Chim. Acta.* **2026**, *589*, 122949. DOI
22. Huang, Y.; Zhang, D.; Baxter, E. T.; et al. Tunable cation coordination by polyoxometalates enables selective heavy metal separation and critical mineral recovery at redox electrochemical interfaces. *Sep. Purif. Technol.* **2026**, *390*, 136885. DOI
23. Lakhanpal, V.; Guillén-Soler, M.; Vilà-Nadal, L.; Long, D.; Cronin, L. Compression of molybdenum blue polyoxometalate cluster rings. *J. Am. Chem. Soc.* **2025**, *147*, 10579-86. DOI PubMed PMC
24. Alizadeh, M.; Yadollahi, B. Synthesis of nanoscale surfactant-encapsulated silica-supported polyoxometalate [Si/AlO_2]@[PWZn]@CTAB and its catalytic application in the oxidation of alcohols. *RSC. Adv.* **2025**, *15*, 8777-83. DOI PubMed PMC
25. Raabe, J.; Jameel, F.; Stein, M.; Albert, J.; Poller, M. J. Heteroelements in polyoxometalates: a study on the influence of different group 15 elements on polyoxometalate formation. *Dalton. Trans.* **2024**, *53*, 454-66. DOI
26. Fu, Y.; Wang, J.; Ma, X.; et al. Ion-exchange strategy for fabricating highly dispersed Co-MoS_2 on N-doped graphene for efficient bifunctional electrocatalytic water splitting. *Int. J. Hydrogen. Energy.* **2024**, *59*, 116-24. DOI
27. Li, W.; Xu, W.; Sun, Z.; et al. A tungsten polyoxometalate mediated aqueous redox flow battery with high open-circuit voltage up to 2 V. *Nat. Commun.* **2025**, *16*, 4654. DOI PubMed PMC
28. Singla, R.; Singh, N.; Pandey, R.; Supriya, S. The photochromism of UiO-66 encapsulated polyoxometalate composites. *ACS. Appl. Eng. Mater.* **2025**, *3*, 2275-87. DOI
29. Feng, L.; Liu, Q.; Xu, G.; et al. Manipulating the dynamic proton transport in electrocatalysis at the nanoscale. *ACS. Catal.* **2025**, *15*, 4394-402. DOI
30. Bibi, R.; Nazir, S.; Shafiq, S.; et al. A novel supramolecular Co-EDTA and Ni-anderson polyoxometalate hybrid as a high-performance electrocatalyst for alkaline water splitting. *Mater. Res. Bull.* **2025**, *186*, 113329. DOI
31. Ma, X.; Xiao, H.; Chen, Y.; Lai, Q.; Li, X.; Zheng, S. Polyoxometalate-based macrocycles and their assembly. *Coord. Chem. Rev.* **2024**, *510*, 215818. DOI
32. Rani, S.; Nadeem, M.; Alrahili, M. R.; et al. Synergistic reductive catalytic effects of an organic and inorganic hybrid covalent organic framework for hydrogen fuel production. *Dalton. Trans.* **2024**, *53*, 10875-89. DOI
33. Schidowski, L.; Friedrich, L. F.; Pawlig, A. H.; Voß, D.; Albert, J. Investigations on the recovery of different structure types of polyoxometalates from aqueous solution using nanofiltration membranes. *ACS. Omega.* **2026**, *11*, 23290-301. DOI PubMed PMC
34. Wang, Z. D.; Yang, Y. Q.; Chen, J. H.; et al. Proton superhighways enabled by hofmeister-electrostatic synergy in all-inorganic polyoxometalate hydrogels for electronics. *Adv. Mater.* **2025**, *38*, e15892. DOI
35. Yuan, X.; Peng, Y.; Zhu, X.; et al. Remote polyoxometalates modulated the d/p-band center proximity in vanadia-based catalyst for simultaneous elimination of NO_x and chlorobenzene. *ACS. Catal.* **2025**, *15*, 7470-81. DOI
36. Blasco-Ahicart, M.; Soriano-López, J.; Carbó, J. J.; Poblet, J. M.; Galan-Mascaros, J. R. Polyoxometalate electrocatalysts based on earth-abundant metals for efficient water oxidation in acidic media. *Nature. Chem.* **2017**, *10*, 24-30. DOI
37. Su, Q.; Liu, Q.; Wang, P.; Ding, J.; Cheng, W.; Huang, Y. Fe doping regulates the surface reconstruction and activates lattice oxygen of NiCr LDH for water oxidation. *Chem. Eng. J.* **2024**, *483*, 149383. DOI

38. Craig, M. J.; Coulter, G.; Dolan, E.; et al. Universal scaling relations for the rational design of molecular water oxidation catalysts with near-zero overpotential. *Nat. Commun.* **2019**, *10*, 4993. DOI
39. Yang, M.; Zhang, C. H.; Li, N. W.; Luan, D.; Yu, L.; Lou, X. W. Design and synthesis of hollow nanostructures for electrochemical water splitting. *Adv. Sci.* **2022**, *9*, 2105135. DOI PubMed PMC
40. Lin, Y. X.; Feng, W. J.; Zhang, J. J.; et al. A polyimide nanolayer as a metal-free and durable organic electrode toward highly efficient oxygen evolution. *Angew. Chem. Int. Ed.* **2018**, *57*, 12563-6. DOI
41. Zhao, N.; Wang, X.; Zhu, S.; et al. Polyoxometalates-derived self-supporting porous micropillar catalysts for efficient overall water splitting. *Inorg. Chem. Commun.* **2026**, *184*, 115939. DOI
42. Yan, Z.; Liu, H.; Hao, Z.; Yu, M.; Chen, X.; Chen, J. Electrodeposition of (hydro)oxides for an oxygen evolution electrode. *Chem. Sci.* **2020**, *11*, 10614-25. DOI PubMed PMC
43. Woods, E. F.; Yan, L.; Lee, J.; et al. Molecular design and redox behavior of polyoxometalates: structure-property insights for flow battery materials. *ACS. Electrochem.* **2026**, *2*, 1038-54. DOI
44. Zhao, Z.; Sui, L.; Wang, Z.; et al. Enhanced electrocatalytic activity of NiCoP/Ni_5P_4@NiFe-LDH catalysts via Ir doping and oxygen vacancy engineering. *Energy. Mater.* **2026**, *6*, 600025. DOI
45. Ahmad, W.; Ahmad, N.; Wang, K.; et al. Electron-sponge nature of polyoxometalates for next-generation electrocatalytic water splitting and nonvolatile neuromorphic devices. *Adv. Sci.* **2023**, *11*, 2304120. DOI PubMed PMC
46. Dashtian, K.; Shahsavarifar, S.; Usman, M.; et al. A comprehensive review on advances in polyoxometalate based materials for electrochemical water splitting. *Coord. Chem. Rev.* **2024**, *504*, 215644. DOI
47. Xu, S. Y.; Shi, W.; Huang, J. R.; et al. Single-cluster functionalized TiO_2 nanotube array for boosting water oxidation and CO_2 photoreduction to CH_3OH. *Angew. Chem. Int. Ed.* **2024**, *63*, e202406223. DOI
48. Rheinländer, P. J.; Herranz, J.; Durst, J.; Gasteiger, H. A. Kinetics of the hydrogen oxidation/evolution reaction on polycrystalline platinum in alkaline electrolyte reaction order with respect to hydrogen pressure. *J. Electrochem. Soc.* **2014**, *161*, F1448-57. DOI
49. Ahmad, M.; Hussain, M. B.; Mushtaq, M. A.; et al. Advances in electrocatalytic hydrogen evolution coupled with alcohol and aldehyde oxidation: mechanistic insights and economic feasibility. *Adv. Mater.* **2025**, *37*, 2502966. DOI
50. Kim, J. H.; Jo, H. J.; Han, S. M.; Kim, Y. J.; Kim, S. Y. Recent advances in electrocatalysts for anion exchange membrane water electrolysis: design strategies and characterization approaches. *Energy. Mater.* **2025**, *5*, 500099. DOI
51. Lokare, V. B.; Ledinic, A.; Wehr, N.; Hohenschutz, M. Hydrogels under superchaotropic control: polyoxometalate stabilization and pH-responsive crosslinking in cellulose ether solutions. *Angew. Chem. Int. Ed.* **2026**, *65*, e6958664. DOI PubMed PMC
52. Ma, T.; Yan, R.; Wu, X.; et al. Polyoxometalate-structured materials: molecular fundamentals and electrocatalytic roles in energy conversion. *Adv. Mater.* **2024**, *36*, 2310283. DOI
53. Gao, D.; Liu, R.; Biskupek, J.; Kaiser, U.; Song, Y. F.; Streb, C. Modular design of noble-metal-free mixed metal oxide electrocatalysts for complete water splitting. *Angew. Chem. Int. Ed.* **2019**, *58*, 4644-8. DOI PubMed
54. Goberna-Ferrón, S.; Vigara, L.; Soriano-López, J.; Galán-Mascarós, J. R. Identification of a Nonanuclear $\{Co^{II}_9\}$ polyoxometalate cluster as a homogeneous catalyst for water oxidation. *Inorg. Chem.* **2012**, *51*, 11707-15. DOI
55. Luo, W.; Hu, J.; Diao, H.; Schwarz, B.; Streb, C.; Song, Y. F. Robust polyoxometalate/nickel foam composite electrodes for sustained electrochemical oxygen evolution at high pH. *Angew. Chem. Int. Ed.* **2017**, *56*, 4941-4. DOI PubMed
56. Feng, Y.; Zhao, M.; Yang, J.; et al. Wearing gigantic silver armor on transition-metal-containing polyoxometalates: formation of supertetrahedral intercluster compounds. *Angew. Chem. Int. Ed.* **2025**, *64*, e202505511. DOI
57. Gutiérrez-Barroso, I.; Quintanilla, K. A.; Martínez, M.; Peña-Cabrera, E.; Galván, A.; Vázquez, M. A. Supported Keggin anion catalyst: a study of its multifunctionality in retro-aldol condensation of 2*H*-chromenes. *Dalton. Trans.* **2026**, *55*, 6148-58. DOI PubMed
58. Li, J.; Yang, M.; Tian, A.; Cao, X.; Ying, J. Synergistic enhancement of nitrate-to-ammonia conversion and supercapacitor performance by binuclear copper-modified Keggin-type polyoxometalate complex. *J. Colloid. Interface. Sci.* **2026**, *709*, 139892. DOI
59. Nowicka, D.; Vadra, N.; Wieczorek-Szweda, E.; Patroniak, V.; Gorczyński, A. Overview of wells-dawson polyoxometalates: from structure and functionalization to application. *Coord. Chem. Rev.* **2024**, *519*, 216091. DOI
60. Asif, H. M.; Bi, R. B.; Tariq, M.; et al. Synthesis and characterization of polyvanadium and heteropoly-tungsten based inorganic wells dawson polyoxometalates hybrids. *Russ. J. Inorg. Chem.* **2021**, *66*, 340-7. DOI
61. Wang, L.; Li, W.; Wu, L.; Dong, X.; Hu, H.; Xue, G. A new polyanion with Dawson-like constitution: $[H_2SeW_{18}O_{60}]^{6-}$. *Inorg. Chem. Commun.* **2013**, *35*, 122-5. DOI
62. Wang, S.; Hwang, J.; Kim, E. Polyoxometalates as promising materials for electrochromic devices. *J. Mater. Chem. C.* **2019**, *7*, 7828-50. DOI
63. Li, J.; Wang, X.; Song, G.; Lin, H.; Wang, X.; Liu, G. Various anderson-type polyoxometalate-based metal-organic complexes induced by diverse solvents: assembly, structures and selective adsorption for organic dyes. *Dalton. Trans.* **2020**, *49*, 1265-75. DOI

64. Huang, S.; Zhou, Q.; Song, Y.; et al. Electronic modulation of Mo=O sites in Anderson POMs: a molecular platform for rational catalyst design in oxidation desulfurization. *Appl. Surf. Sci.* **2026**, *718*, 164988. DOI
65. Wu, P.; Wang, Y.; Huang, B.; Xiao, Z. Anderson-type polyoxometalates: from structures to functions. *Nanoscale* **2021**, *13*, 7119-33. DOI
66. Xu, F.; Han, X.; Xu, R.; et al. Hydrogels with negligible hysteresis, enhanced conductivity, and good absorbability enabled by synergistic chain entanglement and polyoxometalates. *ACS. Appl. Mater. Interfaces.* **2025**, *17*, 70018-28. DOI
67. Yao, S.; Xu, L.; Ding, X.; Yang, W.; Jiang, Z.; Zhan, C. Remodeling behaviors of polyoxometalate in a flexible chiral complex system. *Inorg. Chem.* **2025**, *64*, 9953-60. DOI
68. Yu, Z.; Ma, W.; Xue, E.; et al. Establishing redox flow batteries with polyoxometalate-based redox couples for enhanced hydrogen sulfide splitting. *Sustain. Energy. Fuels.* **2025**, *9*, 3278-82. DOI
69. Allada, G.; Matsa, P. K.; Gogoi, K.; Chakraborty, S. Regulating electronic functionality in lindqvist polyoxometalates: a molecular approach to tunable metal oxides. *Chem. Mater.* **2026**, *38*, 2549-90. DOI
70. Davas, D. S.; Mallick, L.; Gopalakrishnan, D. K.; Chakraborty, B.; Vaitla, J. Strain-induced benzannulation of oxaquadricyclanes promoted by a polyoxometalate photocatalyst. *Angew. Chem. Int. Ed.* **2025**, *64*, e202507189. DOI PubMed
71. Li, C.; Cheng, P.; Sun, Q. Integrating polyoxometalates into discrete coordination assemblies: from synthesis to supramolecular functions. *Coord. Chem. Rev.* **2026**, *559*, 217842. DOI
72. Li, Y.; Qiu, Q.; Fan, S.; et al. A series of rare-earth phosphine-oxygen complexes containing $[PW_{12}O_{40}]^{3-}$ with highly efficient photocatalytic degradation of MB. *CrystEngComm* **2024**, *26*, 5809-19. DOI
73. Liu, Q.; Rabbani, S. M. G.; Hou, Z.; et al. Isolated and H_2-reduced Anderson clusters catalyse low-temperature hydrogenation of CO_2 to methanol. *Nat. Chem.* **2026**, *18*, 1142-50. DOI
74. Du, M. Y.; Xiao, H. P.; Xu, R. F.; et al. A sonosensitive heterometallic polyoxometalate for highly efficient chemo-sonodynamic synergistic cancer therapy. *Angew. Chem. Int. Ed.* **2025**, *64*, e202514859. DOI
75. Kozma, K.; Mpacko Priso, G.; Puiggalí-Jou, J.; et al. Super-reduction of polyoxometalates: unlocking the oxidation state of metalate centers down to (III). *J. Am. Chem. Soc.* **2025**, *147*, 42926-37. DOI
76. Niu, X.; Zhang, C.; Zhang, C.; Gao, M. Adsorption behavior of ZIF composites with different loading methods of lacunary polyoxometalates towards cationic dyes. *CrystEngComm* **2025**, *27*, 6065-73. DOI
77. Raabe, J.; Chitnis, S. S.; Poller, M. J. Synthesis and characterization of Al and Si substituted polyoxometalates. *Dalton. Trans.* **2025**, *54*, 9483-8. DOI PubMed
78. Sachdeva, G.; Maloul, S.; Zolg, J.; et al. Polyoxometalate aerogels formed by organofunctionalized anderson polyoxometalates as low molecular weight gelators. *Adv. Mater. Inter.* **2025**, *12*, e00597. DOI
79. Jiang, J.; Wang, X.; Liu, Y.; et al. Photo-fenton degradation of emerging pollutants over Fe-POM nanoparticle/porous and ultrathin g-C_3N_4 nanosheet with rich nitrogen defect: degradation mechanism, pathways, and products toxicity assessment. *Appl. Catal. B. Environ.* **2020**, *278*, 119349. DOI
80. Wang, T.; Xu, M.; Li, F.; Li, Y.; Chen, W. Multimetal-based nitrogen doped carbon nanotubes bifunctional electrocatalysts for triiodide reduction and water-splitting synthesized from polyoxometalate- intercalated layered double hydroxide pyrolysis strategy. *Appl. Catal. B. Environ.* **2021**, *280*, 119421. DOI
81. Li, G.; Yang, F.; Che, S.; et al. Asphalt induced highly dispersed CoP/MoO_2 heterojunction embedded in porous N-doped carbon for pH-universal water splitting. *Int. J. Hydrogen. Energy.* **2024**, *80*, 440-8. DOI
82. Kou, Z.; Zang, W.; Ma, Y.; et al. Cage-confinement pyrolysis route to size-controlled molybdenum-based oxygen electrode catalysts: from isolated atoms to clusters and nanoparticles. *Nano. Energy.* **2020**, *67*, 104288. DOI
83. Yin, D.; Cao, Y.; Chai, D.; et al. A WO_x mediated interface boosts the activity and stability of Pt-catalyst for alkaline water splitting. *Chem. Eng. J.* **2022**, *431*, 133287. DOI
84. Li, J.; Wang, Y.; Liu, C.; et al. Coupled molybdenum carbide and reduced graphene oxide electrocatalysts for efficient hydrogen evolution. *Nat. Commun.* **2016**, *7*, 11204. DOI PubMed PMC
85. Miao, J.; Lang, Z.; Zhang, X.; et al. Polyoxometalate-derived hexagonal molybdenum nitrides (MXenes) supported by boron, nitrogen codoped carbon nanotubes for efficient electrochemical hydrogen evolution from seawater. *Adv. Funct. Mater.* **2018**, *29*, 1805893. DOI
86. Quirós-Díez, E. P.; Guillén-Soler, M.; Herreros-Lucas, C.; et al. POM-based water splitting catalyst under acid conditions driven by its assembly on carbon nanotubes. *Adv. Mater.* **2025**, e12902. DOI
87. Wang, S.; Cao, Y.; Jia, W.; Lu, Z.; Jia, D. A cage-confinement strategy to fabricate Pt-Mo_6Co_6C heterojunction for highly efficient PH-universal hydrogen evolution. *App. Catal. B. Environ.* **2021**, *298*, 120579. DOI
88. Wang, Y.; Wang, Q.; Wu, J.; et al. Asymmetric atomic sites make different: recent progress in electrocatalytic CO_2 reduction. *Nano. Energy.* **2022**, *103*, 107815. DOI

89. Huang, Z.; Yang, Z.; Hussain, M. Z.; et al. Polyoxometallates@zeolitic-imidazolate-framework derived bimetallic tungsten-cobalt sulfide/porous carbon nanocomposites as efficient bifunctional electrocatalysts for hydrogen and oxygen evolution. *Electrochim. Acta.* **2020**, *330*, 135335. DOI
90. Cao, H.; Wei, T.; Liu, Q.; et al. Hollow carbon cages derived from polyoxometalate-encapsuled metal-organic frameworks for energy-saving hydrogen production. *ChemCatChem* **2023**, *15*, e202201615. DOI
91. Huang, H. H.; Li, W.; Hu, C. C.; Sun, X. Q.; Lu, L. G.; Fan, X. F. Role of bonding filling on HER/OER/ORR multifunctional catalytic activity in transition-metals-doped PdPX (X = S, Se, Te). *Rare. Metals.* **2024**, *43*, 5126-40. DOI
92. Li, Z.; Abbas, F.; Feng, F.; et al. Electronic states modulation of $BiVO_4$ with transition metal-substituted polyoxometalates to activate lattice oxygen mechanism for efficient water oxidation. *J. Am. Chem. Soc.* **2025**, *147*, 39169-80. DOI
93. Xiao, B.; Khan, S. U.; Cui, G.; et al. In situ coupling of MnS-MoS_2 bimetallic sulfide on nickel foam by $[MnMo_9O_{32}]^{6-}$ platform for advanced hydrogen evolution. *Clean. Techn. Environ. Policy.* **2023**, *25*, 2629-38. DOI
94. Zhang, L.; Ding, X.; Cong, M.; Wang, Y.; Zhang, X. Self-adaptive amorphous Co_2P@Co_2P/Co-polyoxometalate/nickel foam as an effective electrode for electrocatalytic water splitting in alkaline electrolyte. *Int. J. Hydrogen. Energy.* **2019**, *44*, 9203-9. DOI
95. Ma, T.; Cao, H.; Li, S.; et al. Crystalline lattice-confined atomic Pt in metal carbides to match electronic structures and hydrogen evolution behaviors of platinum. *Adv. Mater.* **2022**, *34*, 2206368. DOI
96. Yuan, S.; Xu, Z.; Du, H.; et al. Transition metal oxide catalysts for acidic oxygen evolution: current status and key strategies toward efficient PEM water electrolysis. *Adv. Energy. Mater.* **2026**, *16*, e71024. DOI
97. Li, B.; Wang, T.; Xu, M.; et al. Structuring MoO_3-polyoxometalate hybrid superstructures to boost electrocatalytic hydrogen evolution reaction. *Chin. Chem. Lett.* **2025**, *36*, 110467. DOI
98. Huang, B.; Ma, Y.; Xiong, Z.; et al. Polyoxometalate-derived Ir/WO_x/rGO nanocomposites for enhanced electrocatalytic water splitting. *Energy. Environ. Mater.* **2020**, *4*, 681-6. DOI
99. Qiu, Y.; Dai, X.; Wang, Y.; Ji, X.; Ma, Z.; Liu, S. The polyoxometalates mediated preparation of phosphate-modified $NiMoO_{4-x}$ with abundant O-vacancies for H_2 production via urea electrolysis. *J. Colloid. Interface. Sci.* **2023**, *629*, 297-309. DOI
100. Zhang, X.; Gan, Q.; Zhou, P.; Chen, Z.; Zhang, Z.; Lu, G. Boosting strong metal-support interactions between Ru and sodium titanate nanowire for hydrogenolysis of polyolefins under mild conditions. *Appl. Catal. B. Environ. Energy.* **2024**, *344*, 123626. DOI
101. Cui, L. P.; Wang, Y. W.; Yu, K.; Ma, Y. J.; Zhou, B. B. A multi-active site subnano heterostructures catalyst grown in situ POM and $Fe_{0.2}Ni_{0.8}Co_2O_4$ onto nickel foam toward efficient electrocatalytic overall water splitting. *Adv. Funct. Mater.* **2024**, *34*, 2408968. DOI
102. Wang, Q.; Tian, Z.; Cui, W.; et al. Hierarchical flower-like CoS_2-MoS_2 heterostructure spheres as efficient bifunctional electrocatalyst for overall water splitting. *Int. J. Hydrogen. Energy.* **2022**, *47*, 12629-41. DOI
103. Gautam, J.; Liu, Y.; Gu, J.; et al. Fabrication of polyoxometalate anchored zinc cobalt sulfide nanowires as a remarkable bifunctional electrocatalyst for overall water splitting. *Adv. Funct. Mater.* **2021**, *31*, 2106147. DOI
104. Guillen-Soler, M.; Vassilyeva, N. V.; Quirós-Díez, E. P.; Vila-Fungueiriño, J. M.; Forment-Aliaga, A.; Gimenez-Lopez, M. D. C. A hierarchical polyoxometalate/Pd/Mos_2 hybrid: developing an efficient novel bifunctional catalyst for water splitting. *Adv. Sustain. Syst.* **2023**, *8*, 2300607. DOI
105. Ding, M.; Wei, Z.; Zhao, W.; et al. Bimetallic Ni_xCo_xP carbon nanofibers network: solid-solution alloy nano-architecture as efficient electrocatalyst for water splitting. *Green. Chem.* **2024**, *26*, 7789-98. DOI
106. Liu, D.; Xu, G.; Yang, H.; Wang, H.; Xia, B. Y. Rational design of transition metal phosphide-based electrocatalysts for hydrogen evolution. *Adv. Funct. Mater.* **2022**, *33*, 2208358. DOI
107. Zhao, D.; Sun, K.; Cheong, W. C.; et al. Synergistically interactive pyridinic-N-MoP sites: identified active centers for enhanced hydrogen evolution in alkaline solution. *Angew. Chem. Int. Ed.* **2019**, *59*, 8982-90. DOI
108. Liu, B.; Li, H.; Cao, B.; Jiang, J.; Gao, R.; Zhang, J. Few layered N, P dual-doped carbon-encapsulated ultrafine MoP nanocrystal/MoP cluster hybrids on carbon cloth: an ultrahigh active and durable 3D self-supported integrated electrode for hydrogen evolution reaction in a wide pH range. *Adv. Funct. Mater.* **2018**, *28*, 1801527. DOI
109. Jiao, Y.; Yan, H.; Wang, R.; et al. Porous plate-like MoP assembly as an efficient pH-universal hydrogen evolution electrocatalyst. *ACS. Appl. Mater. Interfaces.* **2020**, *12*, 49596-606. DOI
110. Zhao, Y.; Wen, J.; Li, P.; et al. Polyoxometalate derived bimetallic phosphide electrocatalysts for high-efficiency hydrogen evolution reaction. *Inorg. Chem. Front.* **2024**, *11*, 7512-24. DOI
111. Gu, H.; Shi, G.; Chen, H.; et al. Strong catalyst-support interactions in electrochemical oxygen evolution on Ni-Fe layered double hydroxide. *ACS. Energy. Lett.* **2020**, *5*, 3185-94. DOI
112. Jiang, H.; Yu, Y.; Duan, X.; et al. Heterostructured MoO_3 anchored defect-rich NiFe-LDH/NF as a robust self-supporting electrocatalyst for overall water splitting. *Small* **2023**, *20*, 2307797. DOI

113. Loganathan, P.; Sunajadevi, K. R. P.; Muthukumar, D. Keggin-type $H_5PMo_{10}V_2O_{40}$ intercalated MgAl-LDH: structural integrity and bifunctional electrocatalytic activity. *Inorg. Chem.* **2026**, *65*, 4548-68. DOI PubMed
114. Wang, W.; Cai, M.; Wang, T.; et al. Cobalt polyoxometalates anchored on nife-LDH nanoplates as highly active and stable bifunctional catalysts for overall water splitting. *Adv. Mater. Technol.* **2023**, *9*, 2301607. DOI
115. Zhang, J.; Zhang, X.; Ma, Z.; et al. POM-intercalated NiFe-LDH as enhanced OER catalyst for highly efficient and durable water electrolysis at ampere-scale current densities. *ACS. Catal.* **2025**, *15*, 6486-96. DOI
116. Quan, Q.; Li, X.; Song, C.; et al. Polyoxometalate-derived bi-functional crystalline/amorphous interfaces with optimized d-electron configuration for efficient self-powered hydrazine-seawater splitting. *Chem. Eng. J.* **2024**, *488*, 150897. DOI
117. Xia, K.; Yamaguchi, K.; Suzuki, K. Recent advances in hybrid materials of metal nanoparticles and polyoxometalates. *Angew. Chem. Int. Ed.* **2022**, *62*, e202214506. DOI PubMed
118. Li, Y.; Chang, X. R.; Sang, X. J.; et al. Keggin-type polyoxometalate modified Ag/graphene composite materials for electrocatalytic water oxidation. *Eur. J. Inorg. Chem.* **2019**, *2019*, 3597-604. DOI
119. Yue, K.; Lu, R.; Gao, M.; et al. Polyoxometalated metal-organic framework superstructure for stable water oxidation. *Science* **2025**, *388*, 430-6. DOI
120. Yu, T.; Gao, P.; Du, H.; Dong, L. Promoting electrocatalytic water oxidation*via* crafting Co-O-W bridge bonds on an amorphous core/shell NiCo-ZIF@POM catalyst. *Inorg. Chem. Front.* **2024**, *11*, 6661-70. DOI
121. Zhang, J.; Zhang, X.; Fang, K.; et al. Efficient glycerol oxidation on PMo_{12}-encapsulated MOF-74 electrocatalyst coupled with hydrogen evolution at industrial-level current density. *Adv. Funct. Mater.* **2025**, *35*, 2502616. DOI
122. Zeb, Z.; Liu, Y.; Khan, N.; et al. Engineering Mo-doped sulfide heterointerfaces from POM-MOFs for enhanced alkaline seawater hydrogen evolution. *Inorg. Chem.* **2025**, *64*, 24601-14. DOI
123. Lu, Y.; Yue, C.; Li, Y.; et al. Atomically dispersed Ni on Mo_2C embedded in N, P co-doped carbon derived from polyoxometalate supramolecule for high-efficiency hydrogen evolution electrocatalysis. *Appl. Catal. B. Environ.* **2021**, *296*, 120336. DOI
124. He, L.; Huang, S.; Liu, Y.; et al. Multicomponent Co_9S_8@MoS_2 nanohybrids as a novel trifunctional electrocatalyst for efficient methanol electrooxidation and overall water splitting. *J. Colloid. Interface. Sci.* **2021**, *586*, 538-50. DOI
125. Jiao, Y.; Yan, H.; Wang, D.; et al. Multi-touch cobalt phosphide-tungsten phosphide heterojunctions anchored on reduced graphene oxide boosting wide pH hydrogen evolution. *Sci. China. Mater.* **2022**, *65*, 1225-36. DOI
126. Wang, Y.; Wang, T.; Xu, M.; et al. Polyoxometalate superlattices derived bimetallic sulfides to accelerate acidic and alkaline hydrogen evolution reaction. *J. Colloid. Interface. Sci.* **2025**, *679*, 760-8. DOI
127. Qi, Q.; Shao, D.; Zhou, Y.; Wang, Q.; Yu, X. Plasma-induced implanting of active species in metal-organic frameworks for efficient hydrogen evolution reaction. *J. Mater. Chem. A.* **2023**, *11*, 15663-9. DOI
128. Li, S.; Li, J.; Zhu, H.; et al. Development of polyoxometalate-based Ag-H_2 biim inorganic-organic hybrid compounds functionalized for the acid electrocatalytic hydrogen evolution reaction. *Dalton. Trans.* **2023**, *52*, 15725-33. DOI
129. Yue, C.; Sun, F.; Liu, N.; et al. High phase purity of stable 1T-phase Co-doped WS_2 for full pH hydrogen evolution reaction in water and seawater. *Fuel* **2024**, *357*, 129668. DOI
130. Ma, C.; Zhu, S.; Zhao, Y.; et al. CoS_2-MoS_2 nanoflower arrays for efficient hydrogen evolution reaction in the universal pH range. *Langmuir* **2023**, *40*, 744-50. DOI
131. Yang, X.; Cheng, J.; Li, H.; et al. "Tip effect" of hexagram-like Co-doped MoC heterostructure for hydrogen evolution reaction. *Appl. Surf. Sci.* **2023**, *627*, 157284. DOI
132. Liao, M.; Shen, H.; Lin, X.; et al. Interfacial engineering of POM-stabilized Ni quantum dots on porous titanium mesh for high-rate and stable alkaline hydrogen production. *Dalton. Trans.* **2024**, *53*, 5084-8. DOI
133. Sun, F.; Bao, W.; Feng, C.; et al. Construction of ultrafine and highly dispersed $RuSe_2$ on WO_x by "atom-to-cluster" strategy for efficient hydrogen evolution reaction. *Fuel* **2024**, *370*, 131815. DOI
134. Gautam, J.; Kannan, K.; Meshesha, M. M.; et al. Heterostructure of polyoxometalate/zinc-iron-oxide nanoplates as an outstanding bifunctional electrocatalyst for the hydrogen and oxygen evolution reaction. *J. Colloid. Interface. Sci.* **2022**, *618*, 419-30. DOI
135. Kar, A.; Swain, R. K.; Halder, A.; Pradeep, C. P. Self-sulfuration and carbonization of a mixed-metal aryl sulfonium polyoxometalate hybrid: a path to electrocatalytically active ternary composite. *ACS. Appl. Energy. Mater.* **2024**, *7*, 1828-41. DOI
136. Li, B.; Zhang, X.; Hong, L.; et al. Embedded CoMo-POM@IF nanoflower by facile room temperature etching as an enhanced electrocatalyst for oxygen evolution reaction. *Mol. Catal.* **2024**, *564*, 114338. DOI
137. Pathak, N.; Khanam, S. A.; Kim, D.; Park, Y.; Bania, K. K. NiO-Ru/RuO_2@polyoxovanadate for the catalytic MOR and OER in an alkaline medium. *Energy. Fuels.* **2025**, *39*, 4494-506. DOI
138. Wu, Y.; Niu, S.; Wei, Z.; Meng, L.; Wei, W. Steric construction and modulation of Co-N_x single-atom electrocatalysts via polyoxometalate clusters integration. *Appl. Catal. B. Environ. Energy.* **2024**, *352*, 124014. DOI

139. Wang, J.; Ling, Q.; Yao, Y.; et al. Willow catkin-like Co_4S_3-WS_2 nanostructured electrocatalyst for efficient overall alkaline water splitting. *ACS. Appl. Nano. Mater.* **2024**, *7*, 24408-16. DOI
140. Soriano-López, J.; Quirós-Huerta, J.; Seijas-Da, Silva. Á.; et al. Elucidation of the activity and pH stability limits of polyoxometalate-intercalated layered double hydroxide nanocomposites toward water oxidation catalysis. *Inorg. Chem.* **2025**, *64*, 3242-55. DOI PubMed PMC
141. Huang, X.; Kang, H.; Wang, H.; Zhang, D.; Yang, L.; Zhou, Z. Enhanced electrocatalytic capacity of two POM@NH_2-MIL-101(Fe) composites for oxygen evolution reaction. *ChemCatChem* **2024**, *17*, e202401594. DOI
142. Zhao, Y.; Gao, D.; Liu, S.; et al. POM@ZIF derived mixed metal oxide catalysts for sustained electrocatalytic oxygen evolution. *Chem. A. Eur. J.* **2023**, *29*, e202203220. DOI
143. Zubair, M.; Shen, L.; Hyeong Lee, T.; Qian, Y.; Joon Kang, D. Stabilizing polyoxometalate for enhanced OER performance using a porous manganese oxide support. *ChemSusChem* **2025**, *18*, e202402294. DOI PubMed
144. He, P.; Wang, W.; Cai, M.; Hou, S.; Liu, H.; Wang, X. Polyoxometalates-derived lattice-confined atomically dispersed catalysts for water electrolysis. *Nano. Res.* **2026**, *19*, 94908188. DOI
145. Krishnamoorthy, K.; Pazhamalai, P.; Swaminathan, R.; Mohan, V.; Kim, S. J. Unravelling the Bi-functional electrocatalytic properties of $\{Mo_{72}Fe_{30}\}$ polyoxometalate nanostructures for overall water splitting using scanning electrochemical microscope and electrochemical gating methods. *Adv. Sci.* **2024**, *11*, 2401073. DOI PubMed PMC
146. Wang, G.; Li, X.; Wang, J.; et al. Vanadium-modulated molybdenum/nickel-based multi-heterostructures finely tailoring d-band centers for electrocatalytic water splitting. *J. Colloid. Interface. Sci.* **2025**, *693*, 137543. DOI
147. Fang, J.; Qian, X.; Xia, J.; et al. Heterostructure engineering of self-supported bimetallic sulfide as an efficient bifunctional electrocatalyst for overall water splitting. *J. Alloys. Compd.* **2023**, *937*, 168339. DOI
148. Cui, H.; Gong, L.; Wang, J.; et al. POM@TM-MOFs prism-structures as a superior bifunctional electrocatalyst for overall water splitting. *J. Solid. State. Chem.* **2024**, *331*, 124550. DOI
149. Jeon, D.; Kim, D. Y.; Kim, H.; et al. Electrochemical evolution of Ru-based polyoxometalates into Si,W-Codoped RuO_x for acidic overall water splitting. *Adv. Mater.* **2023**, *36*, 2304468. DOI